

4



AFAL-TR-87-066

AD:

AD FILE COPY

Final Report  
for the period  
July 1986 to  
July 1987

# Design of a kW, DC Magnetically Contained Electrothermal Thruster

July 1988

Authors:  
G. R. Seikel  
C. V. Franks

SeiTec, Inc.  
P. O. Box 81264  
Cleveland OH 44181

SeiTec Report 8716  
F04611-86-C-0057

AD-A200 850

Approved for Public Release

Distribution is unlimited. The AFAL Technical Services Office has reviewed this report, and it is releasable to the National Technical Information Service, where it will be available to the general public, including foreign nationals.

Prepared for the:

Air Force  
Astronautics  
Laboratory

Air Force Space Technology Center  
Space Division, Air Force Systems Command  
Edwards Air Force Base,  
California 93523-5000

DTIC  
ELECTE  
NOV 04 1988  
S a D  
H

88 11 5

## NOTICE

When U.S. Government drawings, specifications, or other data are used for any purpose other than a definitely related Government procurement operation, the fact that the Government may have formulated, furnished, or in any way supplied the said drawings, specifications, or other data, is not to be regarded by implication or otherwise, or in any way licensing the holder or any other person or corporation, or conveying any rights or permission to manufacture, use, or sell any patented invention that may be related thereto.

## FOREWORD

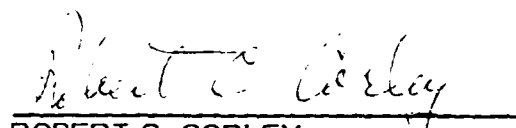
This final report was submitted by SeiTec, Inc., Cleveland, Ohio on completion of contract F04611-86-C-0057 with the Air Force Astronautics Laboratory (AFAL), Edwards AFB, CA. AFAL Project Manager was Lt Terry Sanks.

This report has been reviewed and is approved for release and distribution in accordance with the distribution statement on the cover and on the DD Form 1473.

  
TERRY M. SANKS, 2LT, USAF  
Project Manager

  
CLARENCE J.C. COLEMAN, JR., CAPT, USAF  
Chief, Advanced Concepts Branch

FOR THE COMMANDER

  
ROBERT C. CORLEY  
Deputy Chief, Astronautical Sciences  
Division

## REPORT DOCUMENTATION PAGE

1a. REPORT SECURITY CLASSIFICATION Unclassified		1b. RESTRICTIVE MARKINGS	
2a. SECURITY CLASSIFICATION AUTHORITY		3. DISTRIBUTION/AVAILABILITY OF REPORT Approved for public release; distribution is unlimited.	
2b. DECLASSIFICATION/DOWNGRADING SCHEDULE			
4. PERFORMING ORGANIZATION REPORT NUMBER(S) SeiTec Report 8716		5. MONITORING ORGANIZATION REPORT NUMBER(S) AFAL-TR-87-066	
6a. NAME OF PERFORMING ORGANIZATION SeiTec, Inc.	6b. OFFICE SYMBOL (If applicable)	7a. NAME OF MONITORING ORGANIZATION Air Force Astronautics Laboratory	
6c. ADDRESS (City, State and ZIP Code) P.O. Box 81264 Cleveland, OH 44181		7b. ADDRESS (City, State and ZIP Code) AFAL/ LSVE Edwards AFB, CA 93523-5000	
8a. NAME OF FUNDING/SPONSORING ORGANIZATION	8b. OFFICE SYMBOL (If applicable)	9. PROCUREMENT INSTRUMENT IDENTIFICATION NUMBER F04611-86-C-0057	
8c. ADDRESS (City, State and ZIP Code)		10. SOURCE OF FUNDING NOS.	
		PROGRAM ELEMENT NO. 65502F	PROJECT NO. 3058
		TASK NO. 00	WORK UNIT NO. JT
11. TITLE (Include Security Classification) Design of a kW, DC Magnetically Contained Electrothermal....			
12. PERSONAL AUTHOR(S) Seikel, G.R., and Franks, C.V.			
13a. TYPE OF REPORT Final	13b. TIME COVERED FROM 86JUL TO 87JUL	14. DATE OF REPORT (Yr., Mo., Day) 88/7	15. PAGE COUNT 168
16. SUPPLEMENTARY NOTATION			
17. COSATI CODES		18. SUBJECT TERMS (Continue on reverse if necessary and identify by block number)	
FIELD 21	GROUP 03	SUB. GR. Electric Propulsion; Plasma, Electrothermal; and MPD thrusters. <i>to, ... Thrusters (id)</i>	
19. ABSTRACT (Continue on reverse if necessary and identify by block number) This Phase I SBIR effort included: 1) the engineering design of a kW thruster, 2) the design and/or identification of all the equipment required to test the thruster in Chamber #3 at AFAL, and 3) the fabrication of partial shear and containment coils of the thruster to demonstrate the suitability of their design. The resulting nominal 5 kW, completely magnetically contained thruster design has the potential for long operating life and an overall thrust efficiency between 60 and 80% in the specific impulse range of 2000-3000 seconds, i.e., 50-100% higher efficiency than any existing plasma thruster. This novel thruster concept produces thrust by the expansion of hot plasma in a pair of magnetic nozzles. Upstream containment of the plasma is achieved by a stable, "stellarator" like, magnetic containment system. Plasma heating is accomplished by a DC discharge between the two anodes located inside the magnetic nozzle coils and a downstream hollow			
20. DISTRIBUTION/AVAILABILITY OF ABSTRACT UNCLASSIFIED/UNLIMITED <input type="checkbox"/> SAME AS RPT. <input checked="" type="checkbox"/> OTIC USERS <input type="checkbox"/>		21. ABSTRACT SECURITY CLASSIFICATION Unclassified	
22a. NAME OF RESPONSIBLE INDIVIDUAL TERRY M. SANKS, 2LT, USAF		22b. TELEPHONE NUMBER (Include Area Code) (805) 275-5473	22c. OFFICE SYMBOL LSVE

Block 11 Title Continued.

Thruster (U).

Block 19 Abstract Continued.

cathode which is located on a magnetic field line that passes near the center lines of the anodes. Almost all of the xenon propellant is injected into the discharge through the anodes. The resulting thruster should, based upon the predicted performance, be very attractive for future orbital Air Force electric propulsion applications. The Phase II effort, if funded, would fabricate and test this thruster.



Accession For	
NTIS GRA&I	<input checked="" type="checkbox"/>
DTIC TAB	<input type="checkbox"/>
Unannounced	<input type="checkbox"/>
Justification	
By	
Distribution/	
Availability Codes	
Dist	Avail and/or Special
A-1	

## EXECUTIVE SUMMARY

### SUCCESS STORY

#### Phase I

Objective - Develop the detailed engineering designs of both the required test equipment and a kW completely magnetically contained electrothermal thruster with the potential for long operating life and a thrust efficiency between 60 and 80% in the specific impulse range of 2000-3000 seconds, i.e. 50-100% higher efficiency than any existing plasma thruster.

Approach - SeiTec, Inc.'s novel thruster concept produces thrust by the expansion of hot plasma in a pair of magnetic nozzles. Upstream containment of the plasma is achieved by a stable, "stellarator" like, magnetic containment system. Plasma heating is accomplished by a DC discharge between the two anodes located inside the magnetic nozzle coils and a downstream hollow cathode which is located on a magnetic field line that passes near the center lines of the anodes. Almost all of the xenon propellant is injected into the discharge through the anodes.

Results - The nominal 5kW, xenon propellant thruster design developed under this Phase I effort is substantially more optimized than the prior SeiTec conceptual thruster designs and

should fully meet the Objectives of this project. The design has been independently reviewed by relevant fabrication experts and partial shear and containment coil were fabricated to demonstrate the suitability of their design. All equipment required for testing of the thruster in Chamber #3 at AFAL have also been identified and/or designed.

State-of-the-Art - This novel SeiTec, Inc. thruster directly builds on the best of the past plasma thruster technology: the applied field MPD (Magnetoplasma dynamic) thrusters, but avoids the performance and life limiting problems associated with the physical backplates of these prior thrusters. These prior thrusters had efficiencies in the mid thirty percent range and operating lives of 500 to 1000 hours. Alternative type electric rockets: arcjets and ion thrusters have difficulties in operating in the most desirable specific impulse range for orbital missions.

## Phase II

Based upon the results of the Phase I effort, SeiTec, Inc. feels certain that a Phase II effort could be very successfully accomplished and that the resulting thruster should, based upon the predicted performance, be very attractive for future Air Force electric propulsion applications. A major aerospace subcontractor, the potential Phase III prime contractor, would be used to assist in assessing the thruster's mission potential. No

potential technology barriers can be identified which would prevent successful completion of Phase II.

### Phase III

SeiTec, Inc. envisions that, in Phase III, it would serve as a subcontractor to a major aerospace prime contractor for the development of a multi-kW flight prototype thruster system for future orbital applications. The major applications would be envisioned to be for Air Force missions, but commercial satellite applications may also be attractive. Establishment of the thruster concepts in Phase II should also justify initiation of a MW thruster development/experiment. Novel diffuser concept, to be assessed in the Phase II effort, may also lead to major improvements in test facilities and relatively low cost MW test facilities.

### Summary

This effort should demonstrate a breakthrough improvement in electric thruster technology: plasma thrusters with over 70% efficiency at 2500 seconds, the most attractive specific impulse range for making major mass savings over chemical propulsion for earth orbit missions. This effort is directly aimed at developing a significantly improved multi-kilowatt Air Force space propulsion capability, the scientific basis for future development of a MW

space propulsion capability, and improved test facility designs for electric thrusters. It has no obvious commercial application other than those related to commercial satellite operations in earth orbit or their ground testing.

#### TEAM

All technical effort under this contract was performed by George R. Seikel, the Principle Investigator (PI) and President, SeiTec, Inc. and Clifford V. Franks, Senior Engineer, SeiTec, Inc. The work on plasma probes and thruster physics was reviewed by Dr. Thomas M. York and some management assistance was provided by Mr. Robert M. Purgert, both consultants to SeiTec, Inc.

A team of subcontractors was utilized to fabricate the sample four-turn shear and ten-turn containment coils. The team included N. Noble, Inc. (to EDM the windings); Able Electro-Polishing Co. (to electro-polish the windings); Alloy Bellows, Inc. (to weld the copper shear coil windings); Laser Automation, Inc. (to weld the aluminum containment coil windings); Herron Testing Labs. (to oxidize the sample shear coil); and Anodizing Specialists (to anodize the sample containment coil). In addition, Mr. Keith A. Partee of the Dylon Graphite Company and Mr. Larry R. Mann and his associates of the Union Carbide Corporation, reviewed the design of the graphite nozzle assembly.



## PRESENTATIONS AND PUBLICATIONS

There has been, to date, no public presentation or publication of the results of this contract. The results have only been presented to USAF and other government employees and SeiTec's present and possible future subcontractors. SeiTec, Inc. does, however, anticipate that, at a future date, some of the results contained herein would be included, with acknowledgement of USAF support, in an AIAA publication.

## TABLE OF CONTENTS

	Page
INTRODUCTION	1
THRUSTER PARAMETERS AND PERFORMANCE	7
PARAMETRIC STUDY RESULTS	15
DESIGN OF kW STEADY-STATE, RADIATION- COOLED MAGNETICALLY CONTAINED THRUSTER	23
TEST EQUIPMENT SPECIFICATION AND DESIGN	42
THRUSTER OPERATING PROCEDURE	59
REFERENCES	61
APPENDIX A - THRUSTER PERFORMANCE ANALYSIS	63
APPENDIX B - GENERAL MAGNETIC FIELD CONSIDERATIONS	75
APPENDIX C - MAGNETIC FIELD REQUIREMENTS FOR PLASMA CONTAINMENT	85
APPENDIX D - THRUSTER HEAT BALANCE AND PERFORMANCE CALCULATIONS	91

## LIST OF TABLES

	<u>Page</u>
Table 1 - THRUSTER PARTS LIST	37
Table 2 - SUBCONTRACTORS	40
Table 3 - THRUST STAND PARTS LIST	48
Table 4 - THRUSTER EQUIPMENT	57
Table 5 - THRUST STAND AND DIAGNOSTICS EQUIPMENT	58

## LIST OF FIGURES

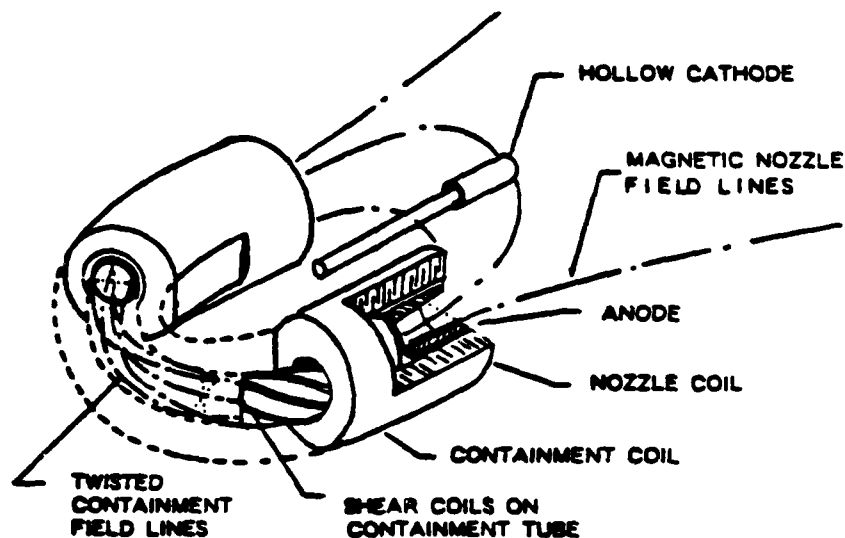
	<u>Page</u>
Fig. 1 - DC Completely Magnetically Contained Thruster Concept.	1
Fig. 2 - Thruster Design Parameters.	8
Fig. 3 - Thruster Mass and Efficiency as a Function of the Minor Radius at which the Containment/Nozzle Coils are Cut Flat.	16
Fig. 4 - Thruster Efficiency as a Function of the Main Discharge Voltage of the Thruster.	16
Fig. 5 - Thruster Mass and Efficiency as a Function of Shear Coil Height.	17
Fig. 6 - Thruster Mass and Efficiency as a Function of Major Radius of the Thruster.	17
Fig. 7 - Thruster Mass and Efficiency as a Function of the Outside Diameter of the Containment/Nozzle Coils.	19
Fig. 8 - Overall Efficiency and Power of the Nominal Thruster Design as a Function of Specific Impulse.	19
Fig. 9 - Variation of Nominal 5 kW Thruster Efficiency and Power as a Function of Containment Field Strength.	20

# LIST OF FIGURES (CONCLUDED)

	<u>Page</u>
Fig. 10 - Variation of Nominal 5 kW Thruster Efficiency and Power as a Function of the Ratio of Plasma to Magnetic Pressure.	20
Fig. 11 - Variation of Nominal 5 kW Thruster Efficiency and Power as a Function of the Ratio of the Radius of Minimum Magnetic Energy Density to the Inside Radius of the Containment Tube.	22
Fig. 12 - 5 kW Thruster.	24
Fig. 13 - 5 kW Thruster Nozzle Assembly Parts.	28
Fig. 14 - Single Turn of Shear Coil.	32
Fig. 15 - Containment and Nozzle Coil Turns.	35
Fig. 16 - Schematic of Thrust Stand.	43
Fig. 17 - NASA LeRC Thrust Stand. Viewed from Flexible Propellant/Water Line Connection Side.	45
Fig. 18 - NASA LeRC Thrust Stand. Viewed from Electrical Connection Side.	46
Fig. 19 - NASA LeRC Thrust Stand with Arcjet Mounted.	47
Fig. 20 - Emmissive Probe.	52
Fig. 21 - Guard Ringed Planer Ion Saturation Probe.	52
Fig. 22 - Electrical Power Schematic.	54
Fig. 23 - Gas System Schematic.	56

## INTRODUCTION

Potential Air Force orbit raising and station keeping missions could be attractively performed with electric propulsion if high efficiency plasma thrusters could be developed in the specific impulse range of 2000 to 3000 seconds. SeiTec, Inc., Ref. 1, has developed a concept for completely magnetically contained electrothermal thrusters which offers the potential of obtaining an efficiency between 60 and 80 percent in the specific impulse range of 2000 to 3000 seconds. The basic concept of these thrusters is that thrust is produced by the expansion of a hot plasma in a pair of magnetic nozzles, as illustrated below.



NOTE: MOST FIELD COILS AND STABILIZING WINDINGS  
OMITTED TO SHOW DETAIL

Fig. 1 - DC Completely Magnetically Contained Thruster Concept

The magnetic containment concept of the thruster uses six shear coil windings in which adjacent windings carry equal and opposite current. These windings produce both a twist in the magnetic containment field lines which is zero on the center line of the toroidal containment tube and increases in magnitude with the value of the distance from the containment tubes center line (i.e. has "shear") and also cause a line of minimum magnetic energy to be created in the center plane of the torus at a fraction of the containment tube's radius inside the containment tube's rear wall. This magnetic field system should provide stable containment for plasmas with pressures up to a number of percent ( $\approx 5\%$ ) of the energy density of the magnetic flux density (B); i.e. its magnetic pressure,  $B^2/2\mu_0$  (where  $\mu_0$  is the permeability of free space).

General considerations regarding the type of magnetic fields in the thrusters are discussed in Appendix B. The specific requirements for plasma containment are discussed in Appendix C.

In this thruster concept, the propellant is introduced into the thruster through small holes in the cylindrical walls of the thruster's physical nozzles, the anodes of a DC thruster. The plasma can conceptually be heated by any method: DC, RF, microwaves, or even by injection of anti-matter. The simplest, lightest, and cheapest method of plasma heating is, however, by a DC discharge; therefore, effort has been concentrated on this

approach.

For DC thrusters, plasma heating is accomplished by a discharge between the anodes located inside the magnetic nozzle coils and a downstream hollow or filament cathode which is located on a magnetic field line that passes near the center lines of the anodes.

This completely magnetically contained thruster concept directly builds on the best of the past magnetoplasma dynamic (MPD) thruster technology: the applied-field thrusters. Since this thruster concept eliminates the physical upstream insulator of prior thrusters it avoids the inefficiencies, operating limits, and life limits associated with backplate wear and erosion in prior thrusters. In addition, this novel concept permits the shape of magnetic nozzles to be optimized to maximize the efficiency of the expansion process.

Conceptional designs of both a kilowatt steady-state thruster and a megawatt quasi-steady thruster were defined in Ref. 1. Analysis, summarized in Appendix A, indicates both have the potential of approaching efficiencies of 80%, at a discharge voltage of 400 to 600 volts. Such an efficiency would be far higher than that available from any alternative electric propulsion system in the 2000 to 3000 second specific impulse range.

Similar analysis of the prior NASA high efficiency (37% at 2200 seconds) downstream cathode MPD thruster indicates that its performance was both directly and indirectly limited by backplate losses. The performance is both directly reduced due to the losses and indirectly reduced by the use of a very rapidly expanding magnetic nozzle field to reduce direct backplate losses, but which is not optimum for the desired expansion process.

The kilowatt thruster can be developed into an attractive low power propulsion system. It uses xenon propellant, a downstream hollow cathode which requires only a few percent of the propellant flow, and a nominal 0.03 tesla containment field. It would operate in a region in which the DC discharge would primarily heat the plasma electrons. As the hot-electron cold-ion plasma expands in the magnetic nozzles of the thruster, the random energy of the electrons will be converted to directed ion energy. This is accomplished by an electric field which the plasma induces in order to maintain its charge neutrality. If the magnetic nozzles are properly shaped, thermal conduction in the electron gas will significantly improve the performance over that which would be obtained with an adiabatic expansion.

The prior megawatt quasi-steady thruster conceptual design was envisioned to be a relatively inexpensive experiment to determine the potential of very-high power thrusters of this type.



An eventual very-high power propulsion system would be envisioned to also operate with similar DC power but would require a high-strength superconducting magnet system, for steady-state operation.

Only one prior steady-state plasma (MPD) thruster which used a superconducting magnetic was ever constructed and tested, Ref. 2. The superconducting magnet of this 25 kW thruster produced a one tesla field in the thruster, and the thruster achieved one of the highest performances measured to date 34% at 2500 seconds. Also, it should be noted that the helium boil-off from superconducting magnet was much less than the thruster's argon propellant flow rate. Recent advances in high temperature superconducting materials may permit future magnets to be directly cooled by the liquid argon propellant.

The prior quasi-steady thruster conceptual design used argon propellant, a downstream hot tungsten filament cathode, and a nominal one tesla magnetic containment field. It would operate in a region in which the DC discharge would primarily heat the plasma ions. The resulting hot-ion cool-electron plasma expansion in the magnetic nozzles of the thruster would be essentially adiabatic.

Both of these prior thruster conceptual designs, in Ref.1, had the same physical size. The 33 times higher strength containment field of the MW thruster, however, gives it over a

thousand times higher magnetic pressure; therefore, it can operate at a thousand times higher plasma pressure and power, if a steady-state design can be defined to handle the thermal heat rejection of losses.

The goal of the subject Phase I SRIR effort was to define an engineering design to the level required for subsequent fabrication and proof-of-concept testing of both a kW thruster and the hardware required to test it. In addition, partial shear and containment coils were fabricated to demonstrate the suitability of their design.

The subsequent sections summarize the design and projected performance of this nominal 5 kW thruster, and the hardware to test it in Chamber #3 at AFAL. In summary, this xenon propellant, 5 kW thruster design is substantially more optimized than the prior, Ref.1, conceptual design and is projected to have an efficiency (including coil power losses) which varies from 69 to 75 percent as specific impulse varies from 2000 to 3500 seconds. At its nominal design xenon propellant flow rate of  $1.2 \times 10^{-5}$  kg/s, it should operate in Chamber #3 at AFAL at a chamber pressure of  $2 \times 10^{-4}$  torr, which should be acceptable for reliable thrust measurements.

## THRUSTER PARAMETERS AND PERFORMANCE

In this Phase I SBIR effort, the determination of the thruster design was accomplished by a process of:

- 1) Improvements in the basic design approach over that of the prior conceptual design, Ref. 1.
- 2) Optimizing in terms of maximizing performance and minimizing mass, the values of appropriate design parameters.
- 3) Compromising the values of other design parameters in terms of a trade-off of thruster performance and mass and of the capability of the thruster to reliably operate at substantially higher than its design shear and containment fields and power level.

The resulting design is not the light-weight flight prototype which would be anticipated to be designed in a potential Phase III effort. The design is, however, a rugged experimental thruster designed for minimum fabrication cost and capable of the wide range of operation needed to establish the feasibility and very-high performance of this novel class of thrusters.

The specific design process consisted of performing a combined thermal power balance and performance analysis for such thrusters. The detailed calculation procedure is summarized in Appendix D. The thruster design and performance parameters are defined in Fig. 2 and in Table D-2.

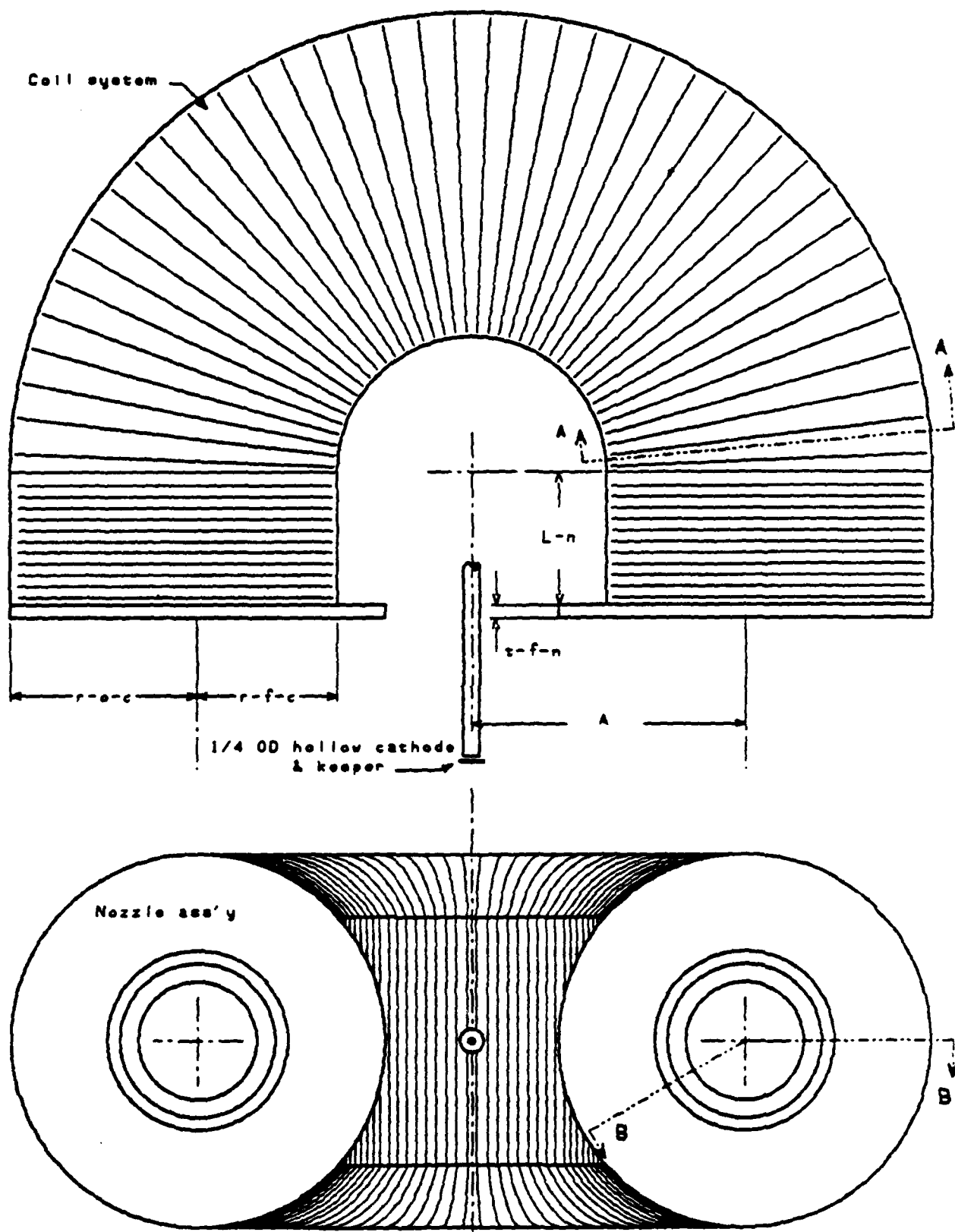
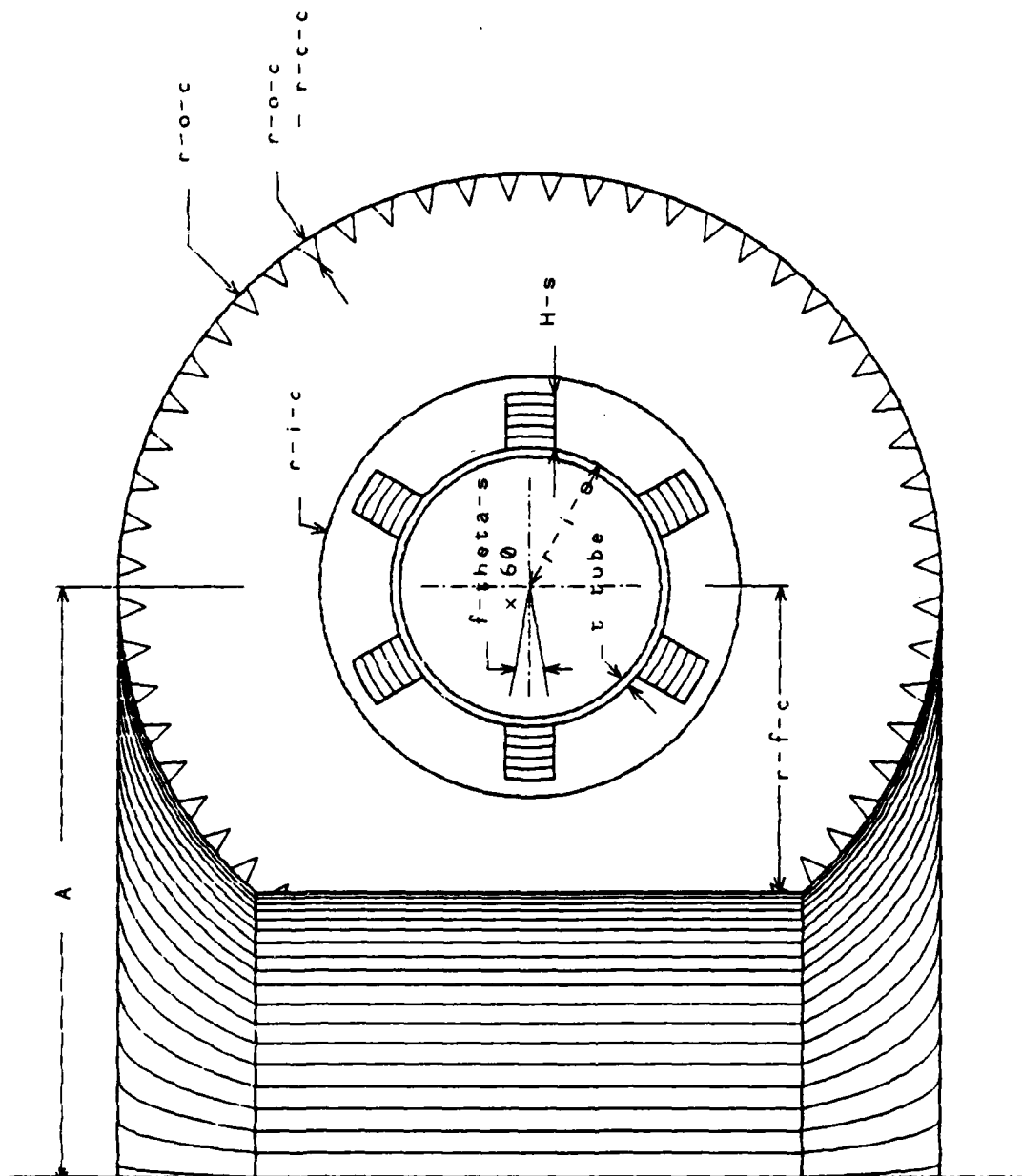
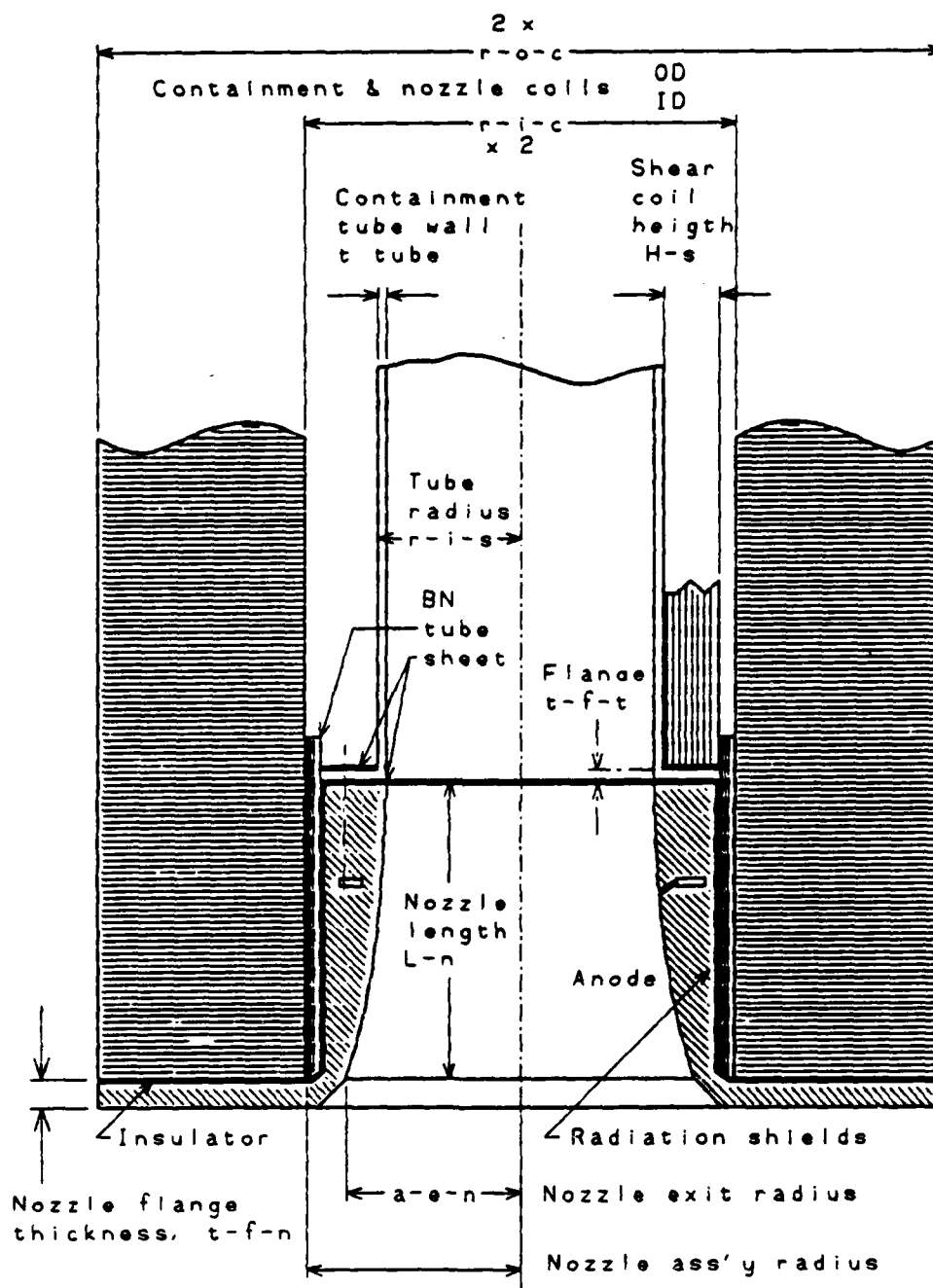


Fig. 2 - Thruster Design Parameters



Section A-A of General Coil System

Fig. 2 - Thruster Design Parameters (continued).



Section B-B of General Thruster

Fig. 2 - Thruster Design Parameters (Concluded)

The approach used assumes:

- 1) The containment tube is constructed by bending an OFHC (oxygen-free high-conductivity) standard thin wall copper tube, selected to be a 2 inch O.D, 0.065 inch wall thickness for the design.
- 2) The power loss in the copper shear coils is radiated to the aluminum containment coils which in turn radiates the sum of the power losses to the test chamber.
- 3) The shear coils are constructed of flat thin OFHC copper strips which are insulated with a very thin coating of  $\text{CuO}$ . Width of the windings is assumed constant with winding radius. Although the top winding will radiate from its surface, this is not considered and all radiation is assumed to be from the two edges of the windings. Crossovers between windings are assumed to have the same width as the windings. However, since all the butt welds required for coil construction will be in the crossovers, the actual width of the crossovers will be increased over that of the windings as an added precaution. The black  $\text{CuO}$  coating on the windings is assumed to provide an emissivity of 0.95. The shear coil windings are assumed to cover one third of the surface of the containment tube and to make one revolution about the minor circumference of the containment tube while traversing the half major circumference of the containment tube.
- 4) The containment and nozzle coils are constructed by lap welding thin high-purity aluminum radial turns to produce an edge wound coil. The coils are insulated by anodizing which can provide an

emissivity of up to 0.8, Ref. 3. It is well known that if one drills a hole with a sufficient L/D in a piece of material the hole will appear black; i.e. have an emissivity of approximately 1. Therefore, to raise the emissivity of the containment coil "V"s have been cut into one half of the outer circumference of the containment coil turns. The number of "V"s used is determined by the amount of overlap of coil turns required for welding and the requirement that the "V" be staggered between turns, so as to form thin deep slots. For the design herein the depth of the "V" was selected to be one half a centimeter which should insure adequate depth for the anticipated coil turn spacing. As illustrated in Fig. 2, sixty such "V"s are cut into each turn of the coil. This design approach should raise the emissivity of tightly packed coils like the nozzle coils up to 0.9. Since the containment coil turns are only tightly packed on their inside major radius, the average spacing between turns for a typical design will be equal to approximately the coil turn thickness. This will further raise the effective emissivity of the coil; therefore, an emissivity of 0.95 has been used in the analysis. Since the nozzle coils have no spacing between the turns and do not have to radiate the power of the shear windings underneath them, they could potentially be constructed with turns having a smaller outside diameter than those of the containment coil. However, because of the uncertainties regarding how well the heat from the anodes can be insulated from these coils and to be conservative, the nozzle coils are assumed to operate at the same temperature as the



containment coil, and the nozzle coil turns are designed to be geometrically similar to the containment coil turns except that their thickness has been increased to account for their closer spacing. The inside diameter of the containment and nozzle coil turns has been selected to be the minimum value that can be assembled over the nozzle structure. The diameter of the nozzle assembly was calculated on the assumption that the nozzle length should be equal to that of the effective radius of the containment coil, this insures that the containment field at lines in the containment tube which have a radius of less than 92% of the inside radius of the containment tube will exit the containment tube without intersecting its walls (see Appendix B-3). The anode exit radius is selected on the basis that the magnetic lines of the containment field that exit the containment tube will exit the anode. Allowing for reasonable thickness of the anode and provisions for thermal and electrical insulation, one concludes that the outside diameter of the anode should be 3 inches for the selective diameter of the containment tube. Allowing for clearance between the containment coil and the nozzle assembly yields, the inside radius of the containment coil is 1.508 inches.

5) The mass of the thruster is calculated on the basis of the mass of all the coil turns plus 10% for structure and the mass of the other major conducting parts: the copper containment tube and its flanges and the nozzles and their flanges, an additional 5% is then added to allow for the other miscellaneous parts. Two materials have been considered for construction of the nozzles and

their flanges: molybdenum and graphite, both materials were considered in the parametric thruster design cases but only the graphite cases are summarized herein. Since graphite permits a lighter thruster and a reliable graphite design appears practical, the final design utilizes this material.

6) Performance of the thruster is calculated based on the approach discussed in Appendix A using the following additional assumptions:

- a) There is no diffusion losses of plasma to the containment tube of the thruster

- b) The magnetic nozzles of the thruster are optimum in shape for the expansion process (as discussed in Appendix B-3)

- c) The efficiency and specific impulse of the thruster include accounting for all the coil power losses and a cathode mass flow loss of 3% of the sum of the anode mass flows.

Appendix D describes the thruster power balance and performance calculations.

## PARAMETRIC STUDY RESULTS

Three important parameters that have a major impact on the thruster's design and performance are the ratio of the radius of minimum magnetic energy to the inside radius of the containment tube ( $\rho$ ), the ratio of the thrusters plasma pressure at the nozzle exit to the magnetic pressure at the exit of the thruster's nozzles ( $\beta$ ), and the magnitude of the maximum center line containment magnetic flux density ( $B_{zo}$ ). The nominal designed conditions for the thruster are:  $\rho = 0.75$ ,  $\beta = 0.05$ , and  $B_{zo} = 0.03T$ . Other values of these three parameters, however, have been explored parametrically. Results of these and some of the other parametric studies are summarized in Figs. 3-11.

Figure 3 illustrates the variation of thruster mass and overall efficiency as a function of the radius at which the containment coils are cut flat while all other parameters are held constant at their design values. Figure 3 illustrates that there is a value of the ratio of this radius, at which the coil turn is cut flat, to the radius to which the containment turn conducts (assumed to be the radius of the bottom of the "V" cuts), which optimizes the thruster efficiency; however, the efficiency optimum is fairly flat and the thruster mass is decreasing with an increasing value of this ratio. Therefore a value of this radius ratio of 0.8 was selected for the thruster design. Note the

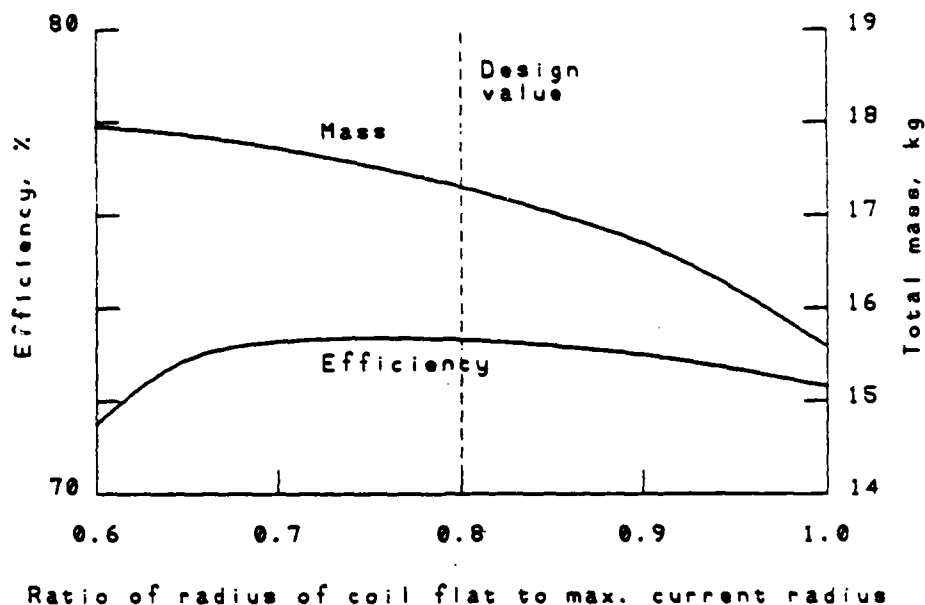


Fig. 3 - Thruster Mass and Efficiency as a Function of the Minor Radius at which the Containment/Nozzle Coils are Cut Flat. Other Parameters Equal to Their Nominal Design Values

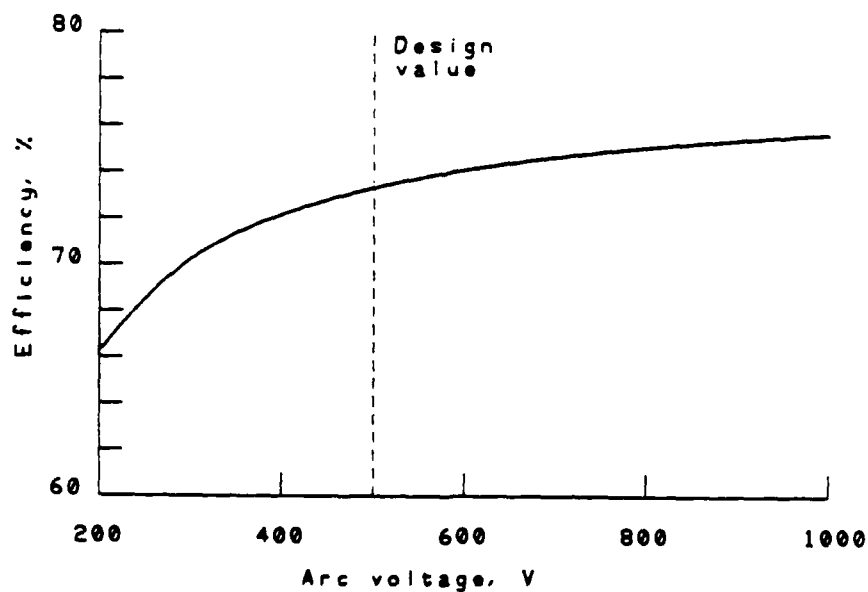


Fig. 4 - Thruster Efficiency as a Function of the Main Discharge Voltage of the Thruster. Other Parameters Equal to Their Nominal Design Values

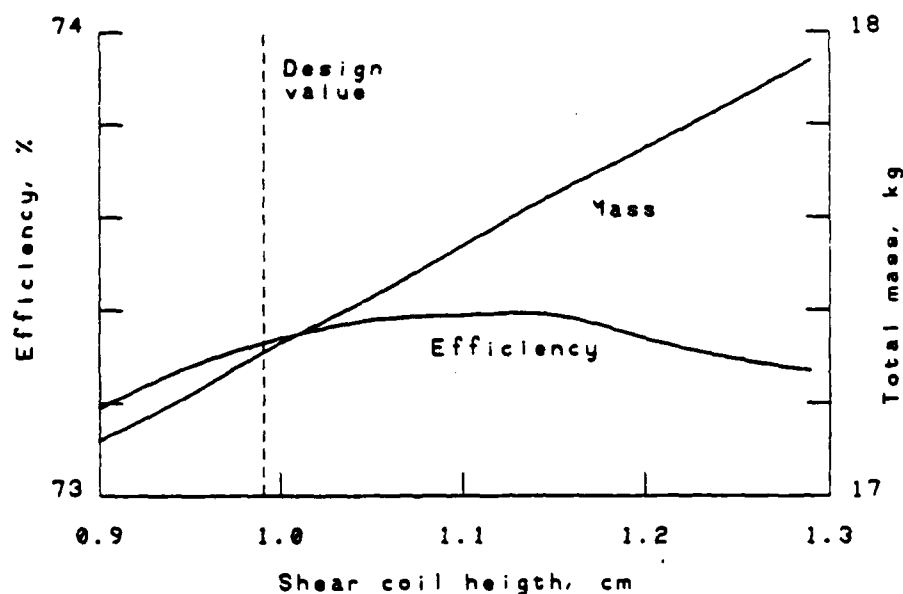


Fig. 5 - Thruster Mass and Efficiency as a Function of Shear Coil Height. Other Parameters Equal to Their Nominal Design Values

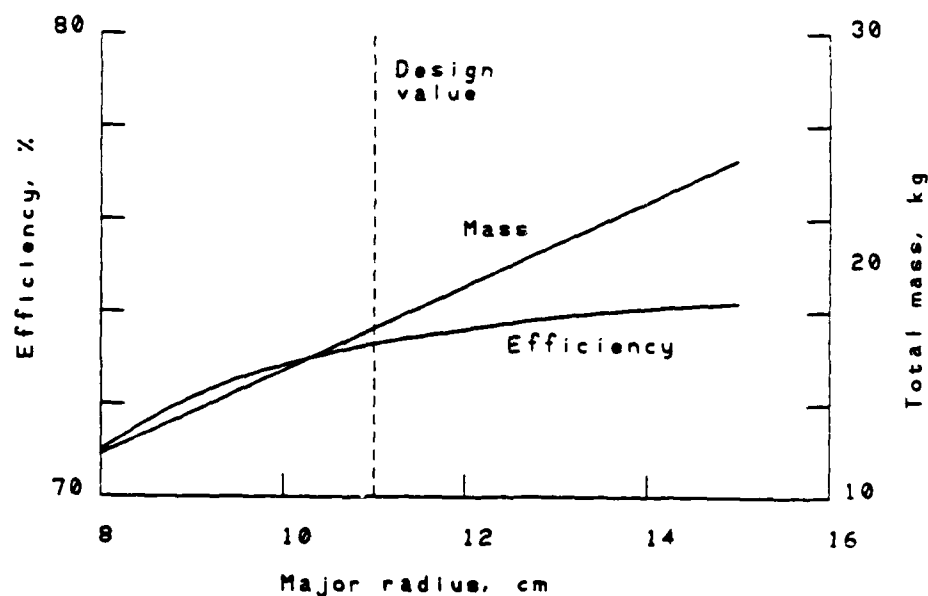


Fig. 6 - Thruster Mass and Efficiency as a Function of Major Radius of the Thruster. Other Parameters Equal to Their Nominal Design Values

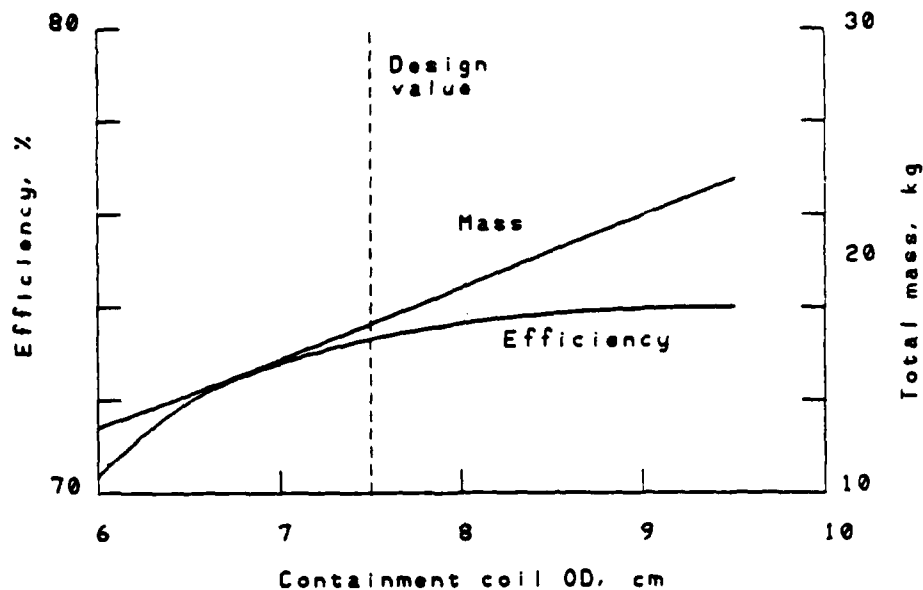
increase in mass with decreasing radius ratio results from the fact that the containment coil turns become more tightly spaced.

Figure 4 illustrates that thruster performance is only a modestly increasing function of discharge voltage in the 500 volt range. Therefore, 500V was selected as the design value of the main discharge voltage.

Figure 5 illustrates that there is a fairly flat optimum in thruster performance and a mass increase with increasing values of the height of the thruster shear coil, H-s.

Figures 6 & 7 illustrate that both thruster performance and mass increase with increasing values of the thrusters major radius, A,; and the outside radius of the containment coil system, r-o-c. Therefore, selection of design values of these parameters is a trade-off of performance and thruster mass. On the basis of the results illustrated in Figs. 5, 6, & 7 and other parametric cases studied, design values of H-s = 0.0099 m, A = 0.11 m and r-o-c = 0.075 m were selected. Note a minimum acceptable value of shear coil height is also desirable to maximize the clearance between the shear and containment coils.

Figure 8 illustrates how the overall thruster efficiency and thruster power level varies as a function of specific impulse for the design values of the thruster's design and operating



**Fig. 7 - Thruster Mass and Efficiency as a Function of the Outside Diameter of the Containment/Nozzle Coils. Other Parameters Equal to Their Nominal Design Values**

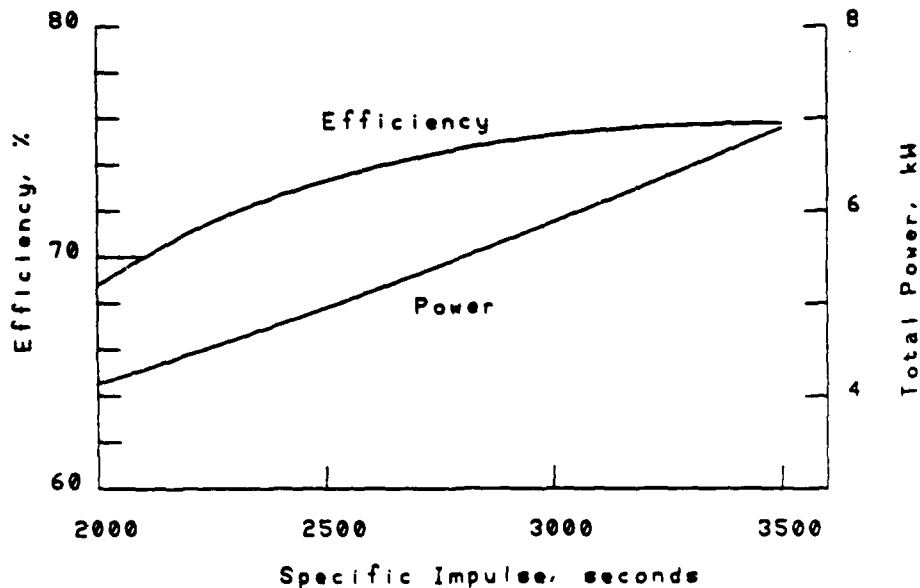


**Fig. 8 - Overall Efficiency and Power of the Nominal Thruster Design as a Function of Specific Impulse.**

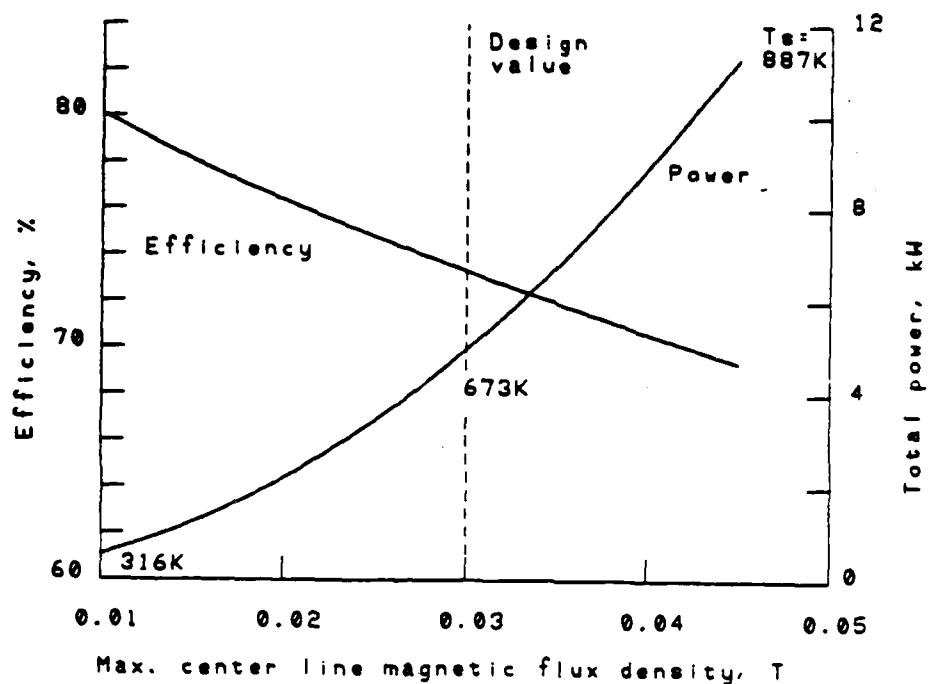


Fig. 9 - Variation of Nominal 5 kW Thruster Efficiency and Power as a Function of Containment Field Strength.

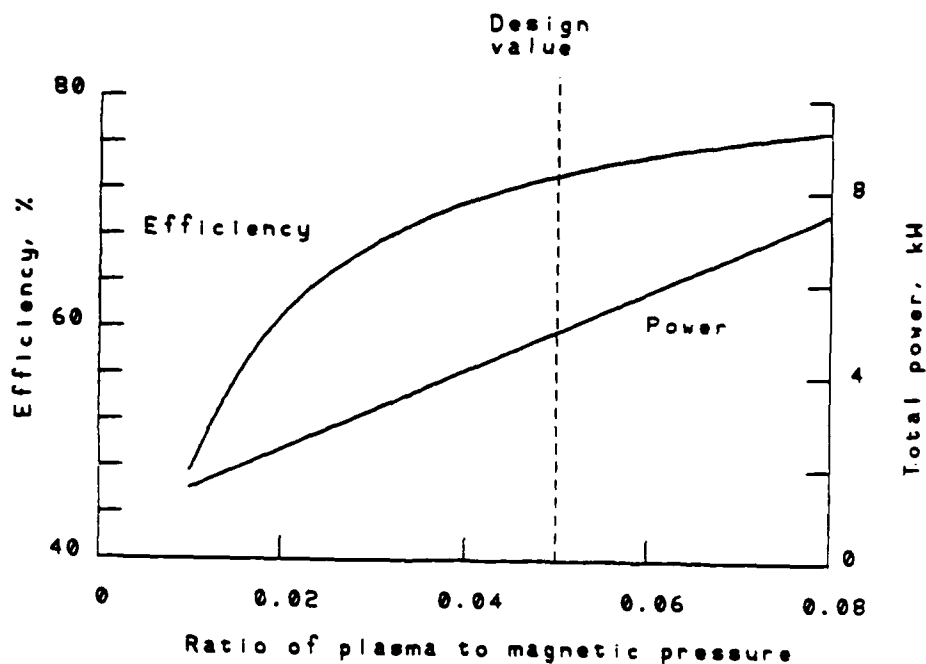


Fig. 10 - Variation of Nominal 5 kW Thruster Efficiency and Power as a Function of the Ratio of Plasma to Magnetic Pressure.



parameters. As indicated the efficiency varies from 69 to approximately 76% as the specific impulse and power level increase from 2000 to 3500 seconds and from 4.1 to 6.9 kW, respectively.

Figures 9, 10, & 11 indicate how the thruster efficiency and power level would vary with variations in the thrusters magnetic field in the beta of the thruster, and in the value of rho. As indicated in Fig. 9, a 50% increase in the containment field of the thruster would double the thruster power level and cause only a modest decrease in the overall efficiency. However, as indicated on the power level variation curve, the shear coil temperature would increase from its design value of 673K to 887K which would be near the operating limit of the coil system.

As shown in Fig. 10, both the thruster performance and power level are strong functions of beta, the ratio of the plasma pressure to the magnetic pressure at the thruster's exit. But based upon past experimental results in the Princeton stellarator, we believe that the 5% design value of beta should be quite realizable.

Figure 11 shows that the thruster performance increases with the value of rho, the radius of minimum energy density to the inside radius of the containment tube. This is due to the decreasing power requirement of the shear coil and as indicated causes the temperature of the shear coil to decrease.

The results of these parametric studies were utilized to define the rugged nominal 5 kW xenon propellant thruster described in more detail in the subsequent sections.

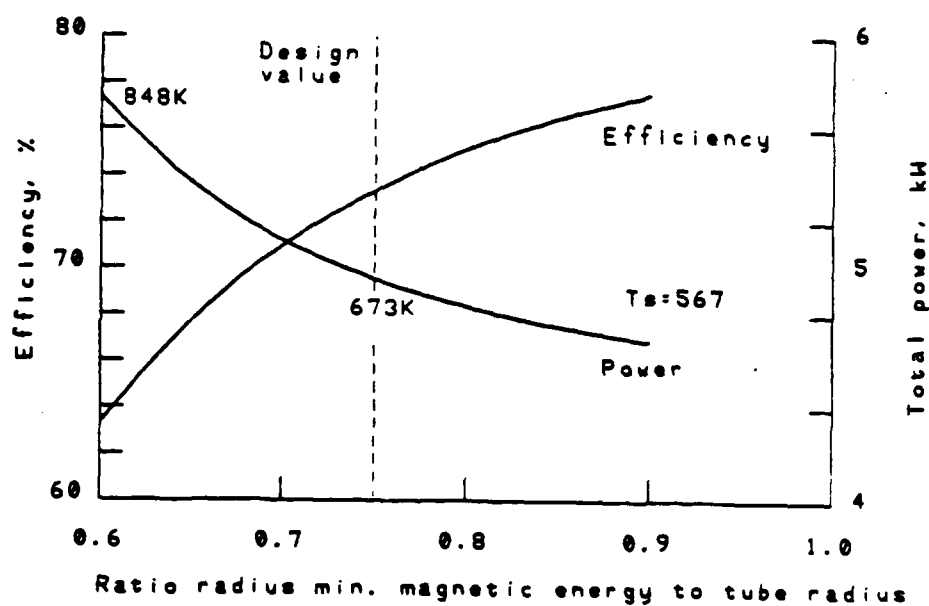


Fig. 11 - Variation of Nominal 5 kW Thruster Efficiency and Power as a Function of the Ratio of the Radius of Minimum Magnetic Energy Density to the Inside Radius of the Containment Tube.

DESIGN OF kW STEADY-STATE,  
RADIATION COOLED-MAGNETICALLY CONTAINED THRUSTER

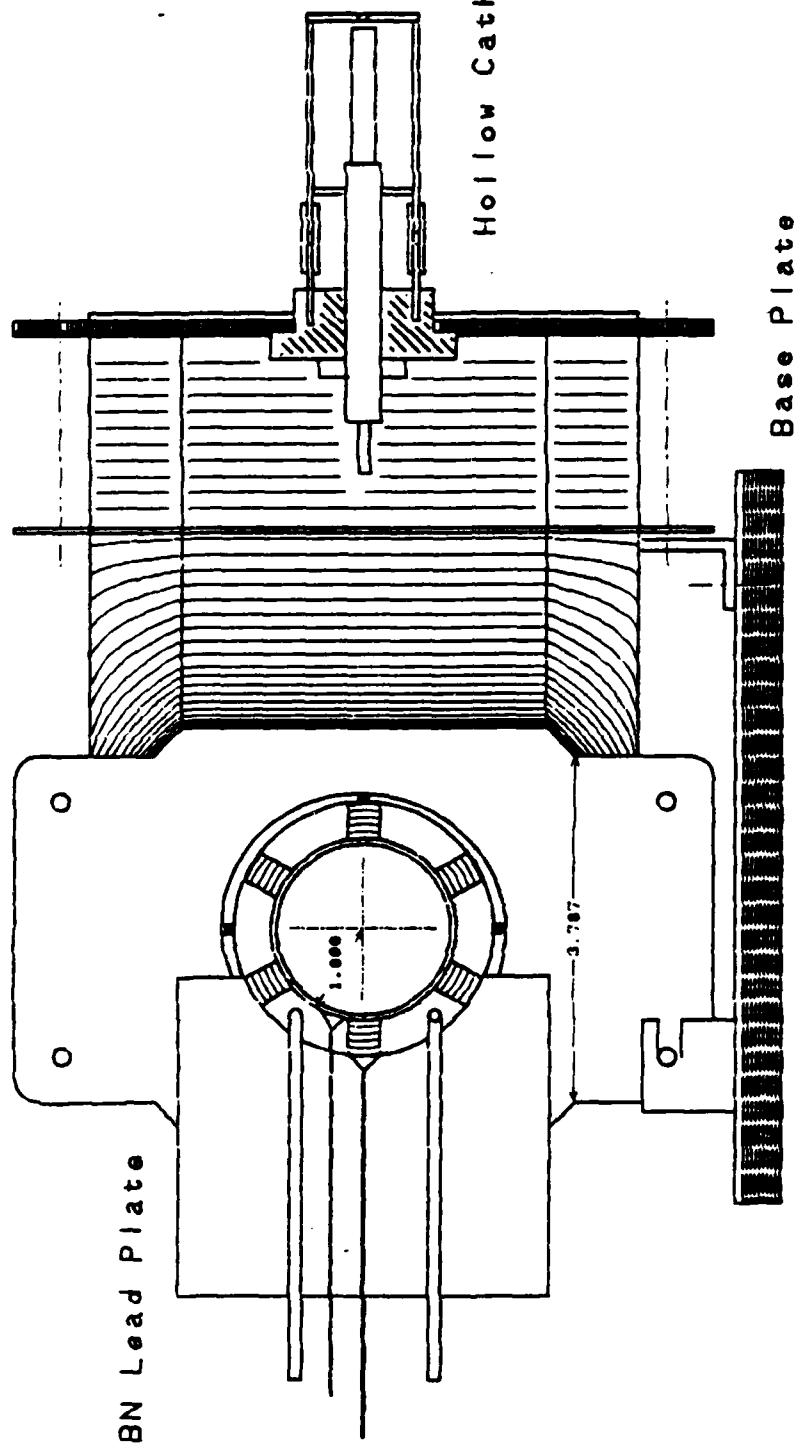
The parameters of the engineering design of the Phase I 5kW thruster were defined by the previously discussed parametric investigations. The engineering design is illustrated in Figure 12. The various sections through the thruster assembly illustrate the details of the design.

The thruster has seven subassemblies: 1) The containment tube assembly, 2) the shear coil assembly, 3) the nozzle assembly, 4) the coil spacer assembly, 5) the containment/nozzle coil assembly, 6) the hollow cathode assembly, and 7) the base plate assembly.

The thruster is constructed about the 2-inch OD containment tube. The containment tube assembly serves to hold the shear coil assembly in place and allow for its leads to exit through the middle of the containment coil of the thruster, along with the anode propellant lines and various thermocouples.

The nozzle assembly bolts to the flange of the containment tube assembly, and the containment and nozzle coils are sized so that they can slide over the nozzles. The coil spacer assembly assures that there is physical isolation between the top of the shear coil and the inside diameter of the containment coil turns.

Containment & Nozzle Coils



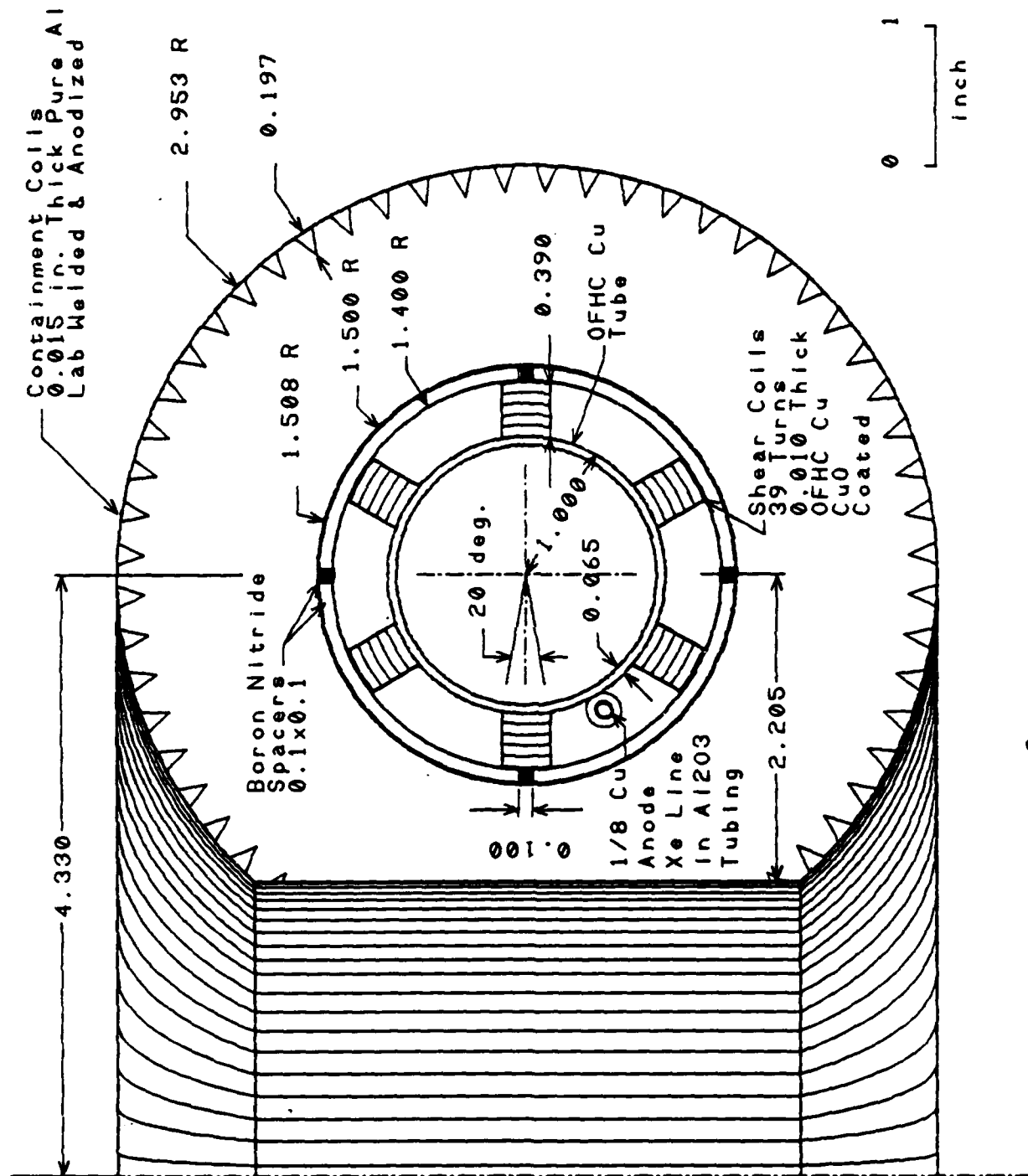
Hollow Cathode Ass'y

Base Plate

BN Lead Plate

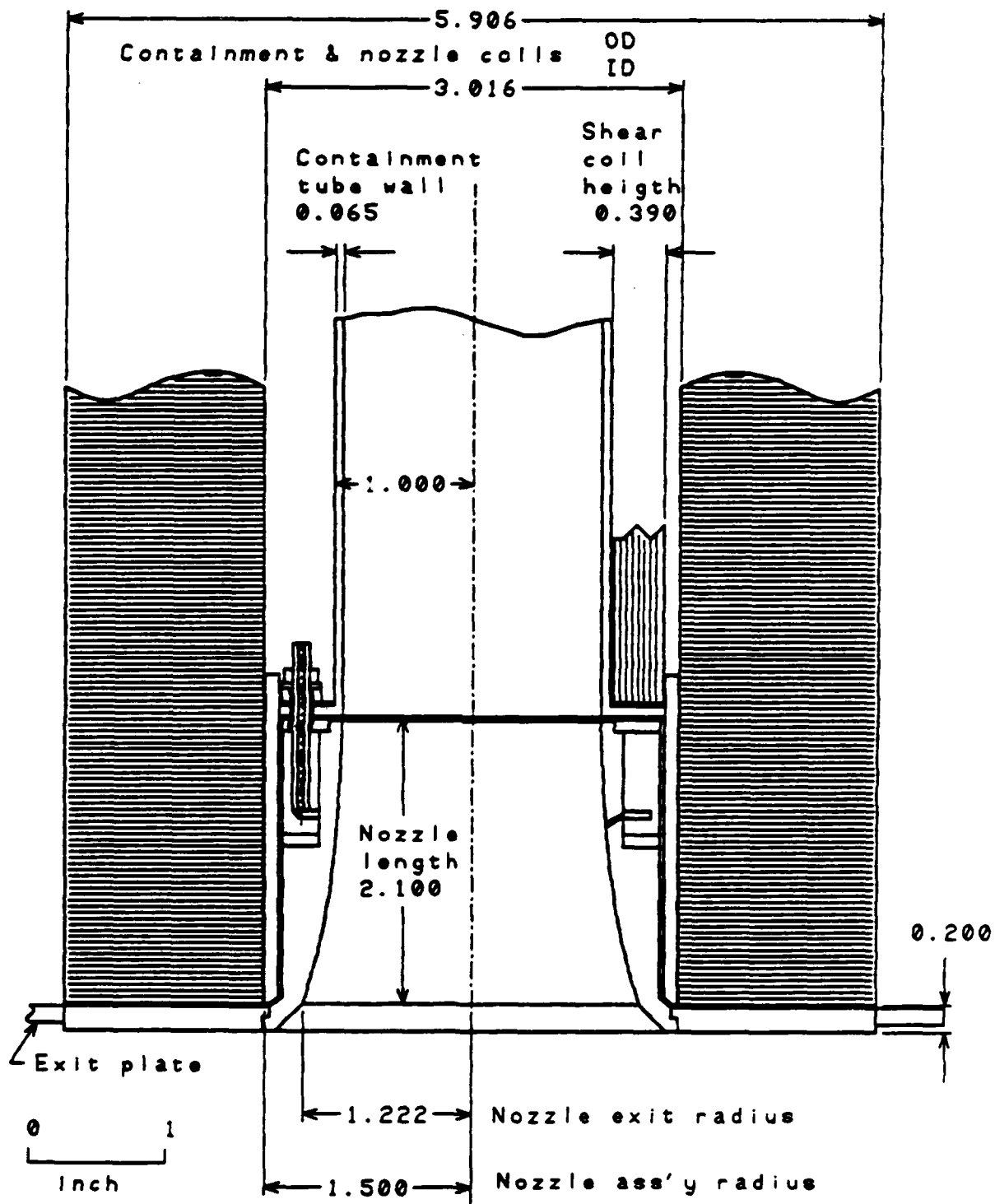
Section thru 5 kW Thruster Center Plane

Fig. 12 - 5 kW Thruster.



Section A-A of 5 kW Thruster Coil System

Fig. 12 - 5 kW Thruster (continued).



Note: See NOZZLE ASS'Y PARTS Dwg. for parts def.

## Section B-B of 5 kW Thruster

Fig. 12 - 5 kW Thruster (concluded)

The flanges and graphite anodes of the nozzle assemblies are used to retain the two halves of the containment/nozzle coil assembly in place. Provisions are made at the middle of the containment coil assembly for differential expansion in the thruster by providing flexible washers at the joint in the assembly at the minimum major radius.

The containment/nozzle coil assembly includes a thruster exit plate which is bolted to the end plates of the nozzle coils. This exit plate of the thruster serves as a mounting plate for the hollow cathode assembly.

The threaded rods connecting the end plates of the nozzle coils and the end plates at the middle of the containment coil also serve to connect the thruster to its base plate. The base plate assembly includes the electrical isolators for the propellant lines and is designed to mount on the thrust stand and to accommodate the thrust stand wiring harnesses and propellant lines.

A listing of all the thruster parts is contained in Table 1, located at the end of this subsection. To more clearly show the parts of the nozzle assembly, an expanded drawing of this assembly is shown in Figure 13.

N01: S.S nut (3req.)  
 N02: S.S washer (3req.)  
 N03: BN spacer (3req.)  
 N04: BN insulator 1

N05A: Ta Tube  
 N05B: Ta stud (2req.)

N06: BN tubing (3req.)

N07: BN Insulator 2

N08: Grafoil seal 1

N09: ATJ graphite  
 ring

N10: Grafoil seal 2

N11: BN tube

Not shown: N12  
 0.0005 Ta radiation shield  
 10 layers between N11 &  
 N08, N09, N10 & N15

N13: Isomica  
 insulator

N14: Flange  
 pyrolytic  
 graphite

N15: ATJ graphite anode

## NOZZLE ASS'Y PARTS

Number Req.  
 per nozzle  
 1 or shown

Ref.: Containment  
 tube ass'y

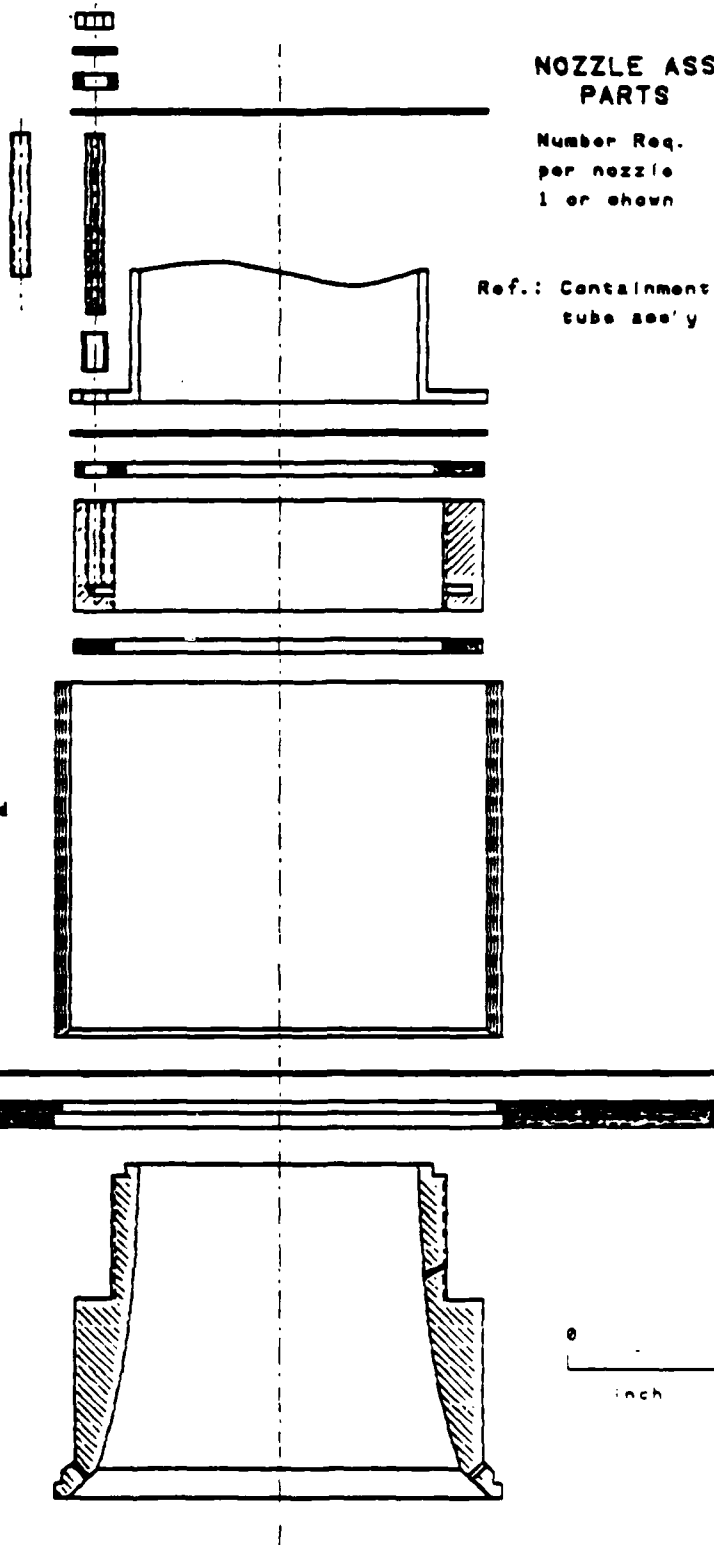


Fig. 13 - 5 kW Thruster Nozzle Assembly Parts



Many parts of the thruster and thrust stand system can be fabricated and/or assembled by a single high quality general machine shop with good welding capabilities, but some other specific parts of the thruster require very specialized capabilities for their fabrication and assembly. These are discussed below.

The containment tube of the thruster will be fabricated by bending a standard thin wall copper tube. SeiTec would utilize a precision bending subcontractor to perform this function and to also bend a three-inch OD tube for use as a containment coil form during its construction.

The assembly and machining of the graphite nozzle assembly also requires a very specialized capability. SeiTec, Inc. would utilize a subcontractor, Dylon Graphite Company, who specializes in graphite fabrication to perform this function. The unique pyrolytic graphite and boron nitride and grafoil parts would be supplied by Union Carbide Corporation. Both of these companies have, at no cost to the government, reviewed SeiTec's design of the nozzle assembly and have indicated its suitability for fabrication.

The fabrication and assembly of the shear coil and containment/nozzle coil assemblies requires a number of unique capabilities which no one subcontractor possesses. To fabricate

the sample four-turn shear coil and ten-turn containment coil, SeiTec, Inc. used the following group of subcontractors, N. Noble, Inc. was used to EDM (Electric Discharge Machine) the shear coil copper windings and the containment and nozzle coil aluminum turns. Able Electro-Polishing Co. was used to electro-polish both the shear coil copper windings and the containment/nozzle coil aluminum turns. Including this process insures that all edges of the windings are well-rounded and that a more reliable layer of thin insulation can subsequently be placed on the various coils. Alloy Bellows, Inc., butt welded the 0.010 inch thick copper shear coil windings. Laser Automation, Inc. lap welded the containment and nozzle coil turns and end plates. The shear coil assembly was insulated by chemically oxidizing it with a thin CuO layer by Herron Testing Laboratories. After welding, the containment coil turns were anodized to insulate them by Anodizing Specialists, Inc. The addresses and contacts for these subcontractors are listed in Table 3.

Fabrication of the refractory metal hollow cathode assembly also requires specialized capability. SeiTec, Inc. would utilize an additional specialized subcontractor to fabricate this assembly.

The final assembly of the total thruster would be performed by SeiTec personnel.

### Shear Coil Assembly

Of particular interest is the design and construction of the shear coil assembly. Figure 14 illustrates the windings of one turn of the 39 turn shear coil. The single line plot illustrates the windings location if the winding had no width, whereas the actual windings will have a width of approximately 0.3 inches and a crossover width of 0.4 inches. From Fig. 14 one can note that a turn of the coil is comprised of only four separate and distinct single windings. This results from the symmetry of the coil construction. Note that the first half winding of the coil turn and the last half winding of the coil turn are geometrically similar and, in fact, are only halves of a complete winding between turns. The second and third windings of the coil are geometrically identical to the second and third from last winding of the turn. The middle winding of the turn is the fourth uniquely shaped winding.

The shear coil is to be fabricated by butt welding the windings near their midpoint in the crossovers between the windings. This allows for easier welding since the winding is straight in the crossovers. In addition, as turns build up on the shear coil, the length of the crossover must be increased for the coil assembly to remain properly stacked. This results from the increase of the minor diameter of the shear coil winding that results from the thickness of the turns. Specifically, the length

THRUSTER SHEAR COIL DESIGN  
Center Line Zero Width Winding  
Starting at Rear Middle of Torus

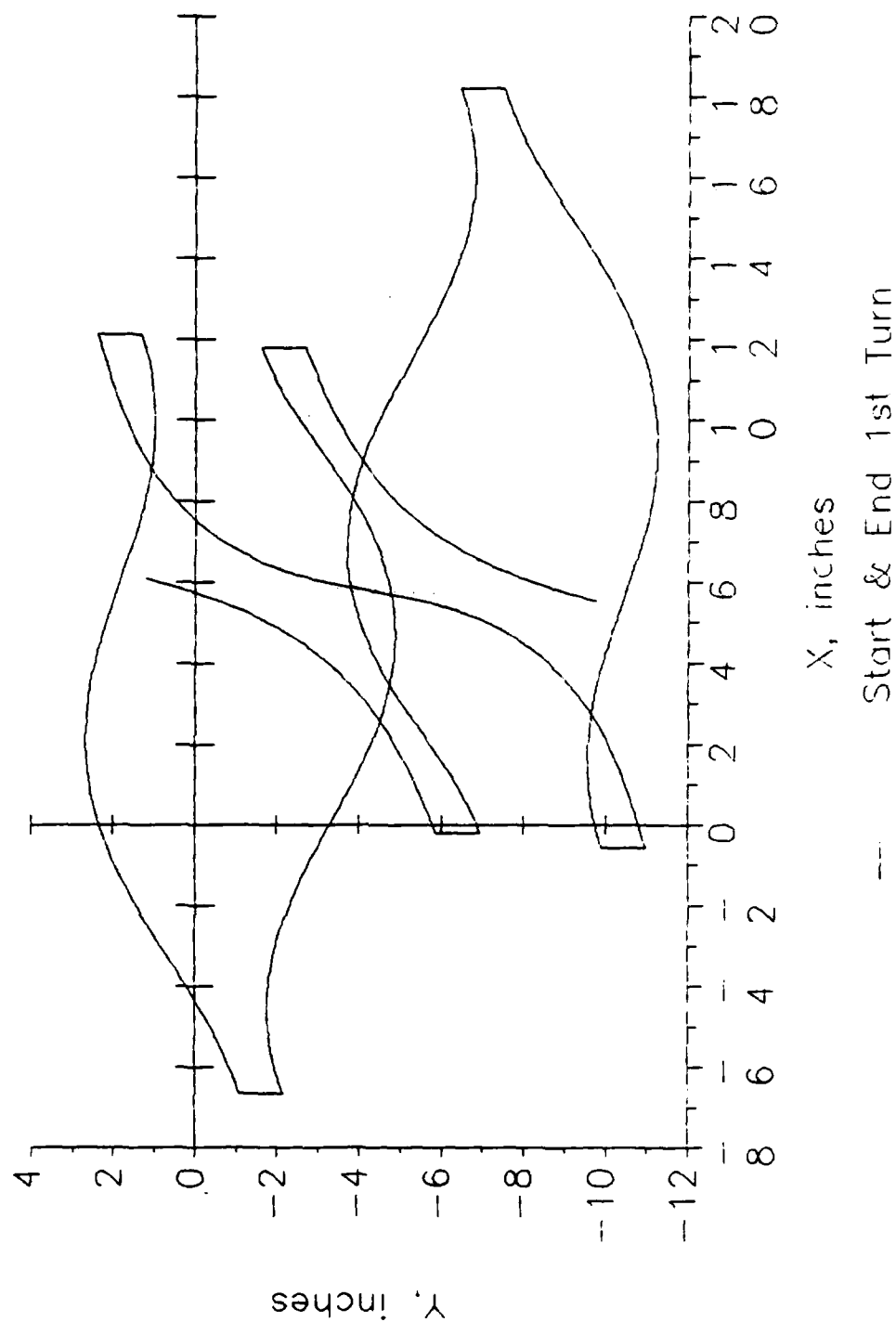


Fig. 14 - Single Turn of Shear Coil.

of the crossovers needs to be increased 0.0105 inches for each added turn.

Buildup of the winding minor diameter also will have some, but a lesser effect, on the desired shape of the winding. Therefore, SeiTec plans to subdivide the shear coil into three sets of windings of 13 turns each. The computer code, developed in this Phase I effort to define the shape of the windings, would be exercised for the mean winding diameter of each of these three groups of windings. The winding crossovers would be designed for the maximum length required for each group of windings. Length of the crossovers would then be trimmed to their appropriate length at the time of welding.

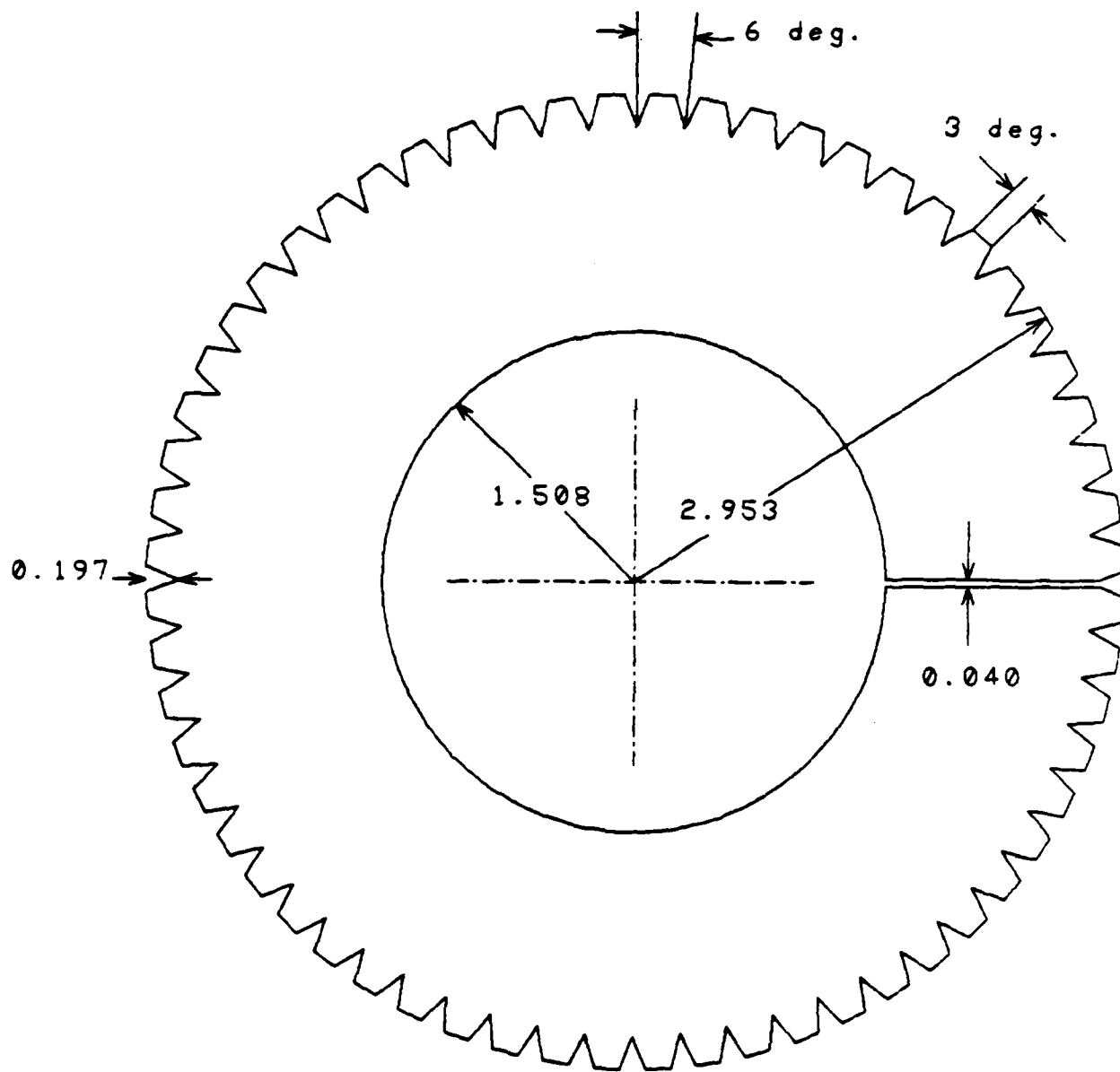
It is desirable to limit the number of different winding shapes since in the EDM machining process all the windings of a specific shape can be simultaneously cut. In addition, there is cost associated with SeiTec, Inc.'s supplying each different winding shape. A computer file on a disk of the required coordinates is utilized by the subcontractor to program the computer controlled wire EDM machine.

#### Containment/Nozzle Coils

All the turns of this coil assembly will initially be cut by wire EDM to have the cross section shown in Fig. 15. The coil

turns are then to be stacked into two stacks which will be the odd and even number turns as one proceeds counterclockwise around the top view of the containment/nozzle coils. As both the odd and even number turns are stacked, each additional turn is rotated so that its radial slit is one tooth (6 degrees) clockwise from the proceeding turn. The coil flat is then cut in the odd number turn stack at an angle which is 3 degrees further clockwise than in the even number turn stack. The turns will be electropolished and then lap welded. If assembled in proper order, the turns will then form the desired assembly.

As was indicated in Fig. 12, the containment/nozzle coil assembly would be fabricated in two halves so that the shear coil leads, propellant lines, and thermocouple leads can exit from its middle outside major diameter. Turns of different thicknesses are required to maintain containment and nozzle fields with approximately uniform ampere-turns per meter. Each half of this assembly will be constructed starting at the middle of the coil with a 0.050 inch thick end plate followed by thirty five-0.010 inch thick turns, followed by one hundred sixty five(165)-0.015 inch thick turns, followed by ten-0.030 inch thick turns, and another 0.050 inch thick end plate and sixty eight-0.030 inch thick turns and a final coil exit 0.050 inch thick end plate. The initial group of 0.010 inch thick turns allows for the space between the two halves of the coil assembly which is required for the leads to exit. The first group of 0.030 inch thick turns



5 kW Thruster Containment Coil Turn

Fig. 15 - Containment and Nozzle Coil Turns.

which are part of the containment and not the nozzle coil are used to compensate for the containment field generated by the crossovers in the shear coil. The 0.030 inch thick turns in the nozzle coil are required to produce with the same current, the same center line ampere-turns per meter as in the containment coil. Thicker turns are required because of the closer packing of the nozzle turns on their centerline.

#### Hollow Cathode

The specific design of a hollow cathode to be used with the thruster is identical to the long-life heaterless cathode developed by NASA Lewis Research Center (LeRC). This is their standard ion thruster hollow cathode with open keeper used for their 30cm ion thruster main cathode. Its minimum breakdown voltage has been experimentally demonstrated to be below 500 volts with xenon. The design has been demonstrated to have an operating life of over 3500 hours with 2000 cycles with a current capability of typically 30 amperes. This significantly exceeds the approximately 9 amperes of current required for nominal design operating conditions of the 5kW thruster.

The cathode design consists of a tantalum tube into which an insert of porous tungsten filled with low work function oxides is inserted. A thoriated tungsten cathode tip is welded to the 1/4-inch OD tantalum tube. The detailed cathode tip hole shape required for long life of the cathode tip hole has been defined by



NASA LeRC. The cathode keeper has a 0.100 inch diameter hole and is spaced 0.060 inches from the face of the cathode.

TABLE 1 - THRUSTER PARTS LIST

Part	Description (Dimensions in Inches)	Req.#	Tot.#
------	------------------------------------	-------	-------

#: 5kT-

CONTAINMENT TUBE ASS'Y

T01	Tube: 20D, 0.065 wall OFHC Cu	1	3
T02	Tube flanges: 2.8 OD, 0.080 thick OFHC Cu	2	3
T03	Studs: 1/8, 3/8 long cu	8	10
T04	Retainers (shear coil) : BN	6	6
T05	Brackets (lead plates) : BN	2	2
T06	Lead plates 1 : 1/4 thick BN	2	2
T07	Lead plates 2 : 1/4 thick BN	2	2
T08	Washers: 1/8 cu	8	12
T09	Nuts: 1/8 cu	8	12
T10	Thermal couples, leads & insulation	4	8
T11	Lead: 14 gage cu	1	-
T12	Xe lines: 1/8 cu	2	-
T13	Anode line insulators: $Al_2O_3$ tubing ass'y	2	-
T14	Fittings: 1/8 female	4	-

SHEAR COIL ASS'Y

S01A	Winding 1: 0.010 thick OFHC Cu, turns 1-13	14	35
B	turns 14 - 26	13	35
C	turns 27 - 39	14	35
S02A	Winding 2: 0.010 thick OFHC Cu, turns 1-13	26	35
B	turns 14 - 26	26	35
C	turns 27 - 39	26	35
S03A	Winding 3: 0.010 thick OFHC Cu, turns 1-13	26	35
B	turns 14 - 26	26	35
C	turns 27 - 39	26	35
S04A	Winding 4: 0.010 thick OFHC Cu, turns 1-13	13	35
B	turns 14 - 26	13	35
C	turns 27 - 39	13	35
S05	Tab: 0.010 thick OFHC Cu	1	1
S06	Leads: 14 gage Cu	2	-

NOZZLE ASS'Y

N01	S.S Nuts: 1/8	6	-
N02	S.S Washers: 1/8	6	-

TABLE 1 - THRUSTER PARTS LIST CONTINUED)

Part	Description (Dimensions in Inches)	Req.#	Tot.#
#: 5kT-			
NOZZLE ASS'Y (CONCLUDED)			
N02	Space: BN	6	8
N04	Insulator 1: 0.020 thick, BN	2	2
N05A	Ta tube: 1/8	2	4
N05B	Ta studs: 1/8	4	6
N06	BN Tubing	6	8
N07	Insulator 2: 0.020 thick BN	2	2
N08	Grafoil seal 1	2	4
N09	ATJ Graphite ring	2	4
N10	Grafoil seal 2	2	4
N11	BN tube: 3 OD	2	2
N12	Radiation shield: 0.0005 Ta	2	5
N13	Isomica insulator: 0.020 thick	2	6
N14	Flange: 0.200 thick pyroytic graphite	2	4
N15	ATJ graphite anodes	2	4
COIL SPACER ASS'Y			
B01	Outside spacers: BN	2	4
B02	Middle spacers: BN	2	4
B03	Inside spacer: BN	1	2
B04	Spacer rings: 3 OD BN	8	16
CONTAINMENT / NOZZLE COIL ASS'Y			
C01A	Turn: 0.015 thick A1	330	400
B	0.030 thick A1	156	200
C	0.010 thick A1	70	100
C02	End plates: 0.050 thick A1	6	10
C03	Coil tabs: 0.015 A1	4	4
C04	Exit plate: 1/8 thick Glastic SG200	1	1
C05	Nozzle rods: 1/8 A1	8	10
C06	Rear rods: 1/8 A1	2	3
C07	Rear inside bolts: 1/8 A1	2	3
C08	Rear spacer: BN	2	2
C09	Flex washers	2	6
C10	BN washers (same as N03)	32	40
C11	BN tubing (same as N06)	16	20
C12	Washers: 1/8 A1	70	-
C13	Nuts: 1/8 A1	28	-
C14	Thermal couples & leads	2	4
C15	Leads	8	4

TABLE 1 - THRUSTER PARTS LIST (CONCLUDED)

Part	Description (Dimensions in Inches)	Req.#	Tot.#
#: 5kT-			
HOLLOW CATHODE ASS'Y			
H01	Ta tube: 1/4 OD	1	3
H02	Inseert: oxide filled porus W	1	2
H03	Cathode tip: W	1	3
H04	Keeper: W	1	3
H05	Support tube: 3/8 Cu	1	1
H06	Support rods: W	2	2
H07	Spacers: BN	2	2
H08	Mount: BN	1	1
H09A	Fittings : male	1	-
B	female	2	-
H10	Tubing: 1/8 Cu	1	-
H11A	Washers: 3/8	2	-
B	1/8	8	-
H12A	Nuts: 3/8	4	-
B	1/8	12	-
H13	Bolts: 1/8	4	-
H14	Leads: Cu	2	-
BASE PLATE ASS'Y			
P01	Plate: 1/4 Glastic SG200	1	1
P02	Feet	4	4
P03A	Thruster mounts: front	2	2
B	rear	2	2
P04	Isolator bodies: BN	3	3
P05	Isolator tubing: $Al_2O_3$	15	-
P06	Isolator screens: S.S	18	-
P07	Isolator flanges: S.S	6	8
P08	O rings	6	12
P09	Fittings: 1/8 male	6	-
P10	Termination strips (6 terminals)	5	-
P11	Isolator bolts: 1/8 ss	12	-
P12	Isolator mounting bolts: 1/8 ss	6	-
P13	Misc. mounting bolts: 1/8 ss	22	-
P14	Washers: 1/8	80	-
P15	Nuts: 1/8	40	-

TABLE 2 SUBCONTRACTORS

DESCRIPTION/SUBCONTRACTOR

---

1. Fabricate pyrolytic graphite, pyrolitic boron nitride, and grafoil nozzle parts.

Union Carbide Corporation  
Specialty Products Group  
P.O. Box 94637  
Cleveland, OH 44101

Larry R. Mann, (216) 529-3959

2. Nozzle assembly and machining

Dylon Graphite Company  
120 First Avenue  
Berea, OH 44017

Keith A. Partee, (216) 234-1600

3. EDM: a) shear coil copper  
b) containment coil aluminum

N. Noble, Inc.  
1650 Collamer Road  
Cleveland, OH 44110

Thomas Delfosse, (216) 761-2133

4. Electropolish: a) shear coil windings  
b) containment & nozzle turns

Able Electro-Polishing Co.  
2904 W. 26 Street  
Chicago, IL 60623

John S. Glass, (312) 847-1631

5. Weld Cu shear coil and containment tube assemblies

Alloy Bellows, Inc.  
18125 Roseland Road  
Cleveland, OH 44112

Robert E. Danielson, (216) 486-3990

TABLE 2 SUBCONTRACTORS (CONCLUDED)

DESCRIPTION/SUBCONTRACTOR

6. Weld containment and nozzle coil turns

Laser Automation, Inc.  
10357 Kinsman Road  
P.O. Box 373  
Newbury, OH 44065

Daniel A. Piscura, (216) 543-9291

7. Oxidize shear coil

Herron Testing Labs.  
5405 E. Schaaf Road  
Cleveland, OH 44131

George Steuber  
Charles J. Belle, (216) 524-1450

8. Anodize containment & nozzle coils

Anodizing Specialists  
7471 Tyler Blvd.  
Mentor, OH

(216) 951-0257

## TEST EQUIPMENT SPECIFICATION AND DESIGN

### THRUST STAND

The thrust stand design selected for use in performance testing of the thruster is a slightly modified version of the compact displacement type thrust stand developed by NASA Lewis Research Center. A simplified schematic of the design is shown in Fig. 16. Pictures of the NASA stand are shown in Figs. 17, 18, and 19. This stand design uses upright flexures to provide the restoring force. The displacement is measured with a linear variable differential transformer (LVDT) over an active range of 5 mm (0.2 inches). The design has very small friction forces that result in no measurable hysteresis. The design makes use of an active damping system which uses the time derivative of the displacement signal as input to an electric forcing coil system which resists thrust stand motion. Although vibrations are typically present in vacuum facilities, the NASA Lewis experience has shown that in their facilities the amplitude of the vibrations was orders of magnitude less than the full-scale thrust stand displacement and did not require filtering of the thrust output signal.

To prevent thermal drift of the stand, the design provides for cooling water to vulnerable parts of the thrust stand assembly. The thruster mounting column includes a water cooled

coil which prohibits heat flow from the thruster back to the stand. The thermal radiation from the thruster is blocked by a cooled water enclosure which surrounds the entire assembly. As a result of these precautions, thermal drift in thrust measurements has not been detected by NASA LeRC. Cooling water and propellant

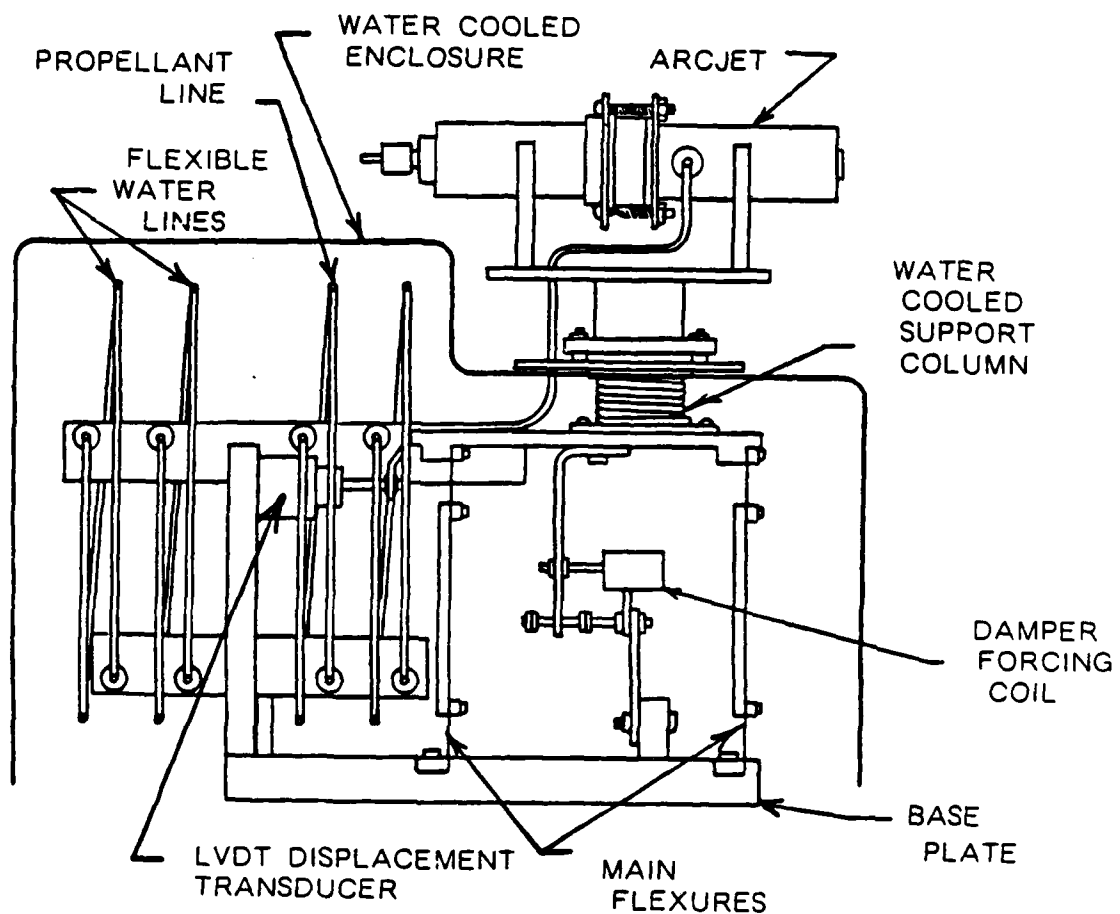


Fig. 16 - Schematic of Thrust Stand.

is brought onto the stand through a flexible feed tubing arrangement. Stand design modification which SeiTec will make include providing for three rather than two propellant feedlines to the stand. The NASA design provides for only manual stand leveling and in situ calibration. Two additional SeiTec design modifications will be to provide for remote in situ stand leveling and remote in situ calibration.

Calibration is carried out by loading the thrust stand with free hanging weights attached to a fine monofilament thread. The weights pull on the stand through a pulley system. NASA has found that this calibration technique has proven to be repeatable to within 1% and simple to use. The planned modification to remotely operate the calibrations system would include adding a weight take-up drum position indicator. By using the weight take-up drum position as X input to an X-Y plotter and the LTDV output as the Y inputs one obtains a system where repeatability of the calibration can be readily checked and compared with previous calibrations. Other modifications to be made to the NASA thrust stand design would be to include the addition of: 1) wheels which would mate with a rail assembly which would be installed in Chamber 3 at AFAL and 2) a thrust stand cart assembly onto which the thrust stand could be rolled directly from the rails in the vacuum tank. A list of the thrust stand parts is shown in Table 2. Drawings of the various thruster parts have been furnished to SeiTec by NASA LeRC.



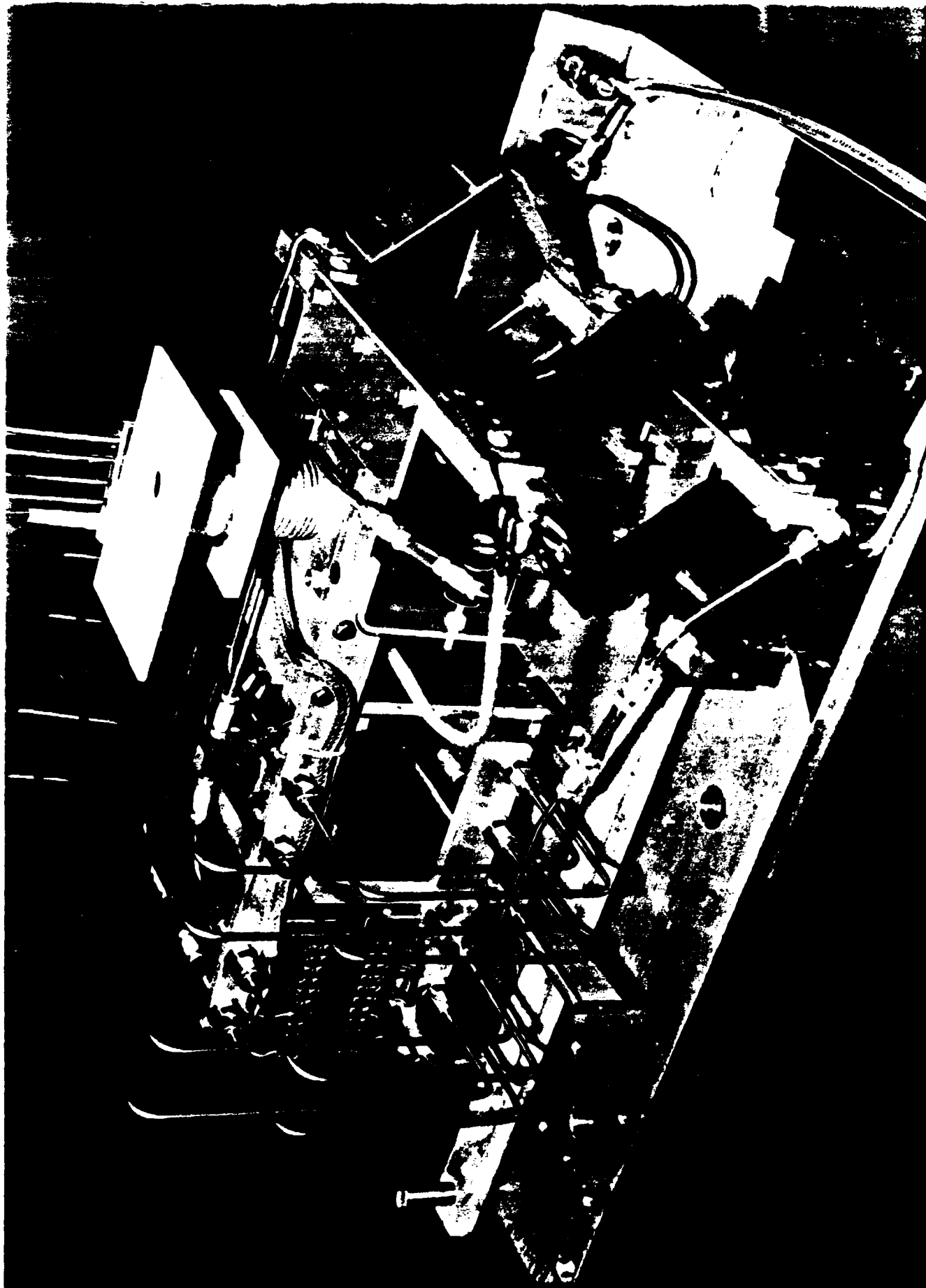


Fig. 17 - NASA LeRC Thrust Stand. Viewed from Flexible Propellant/Water Line Connection Side.

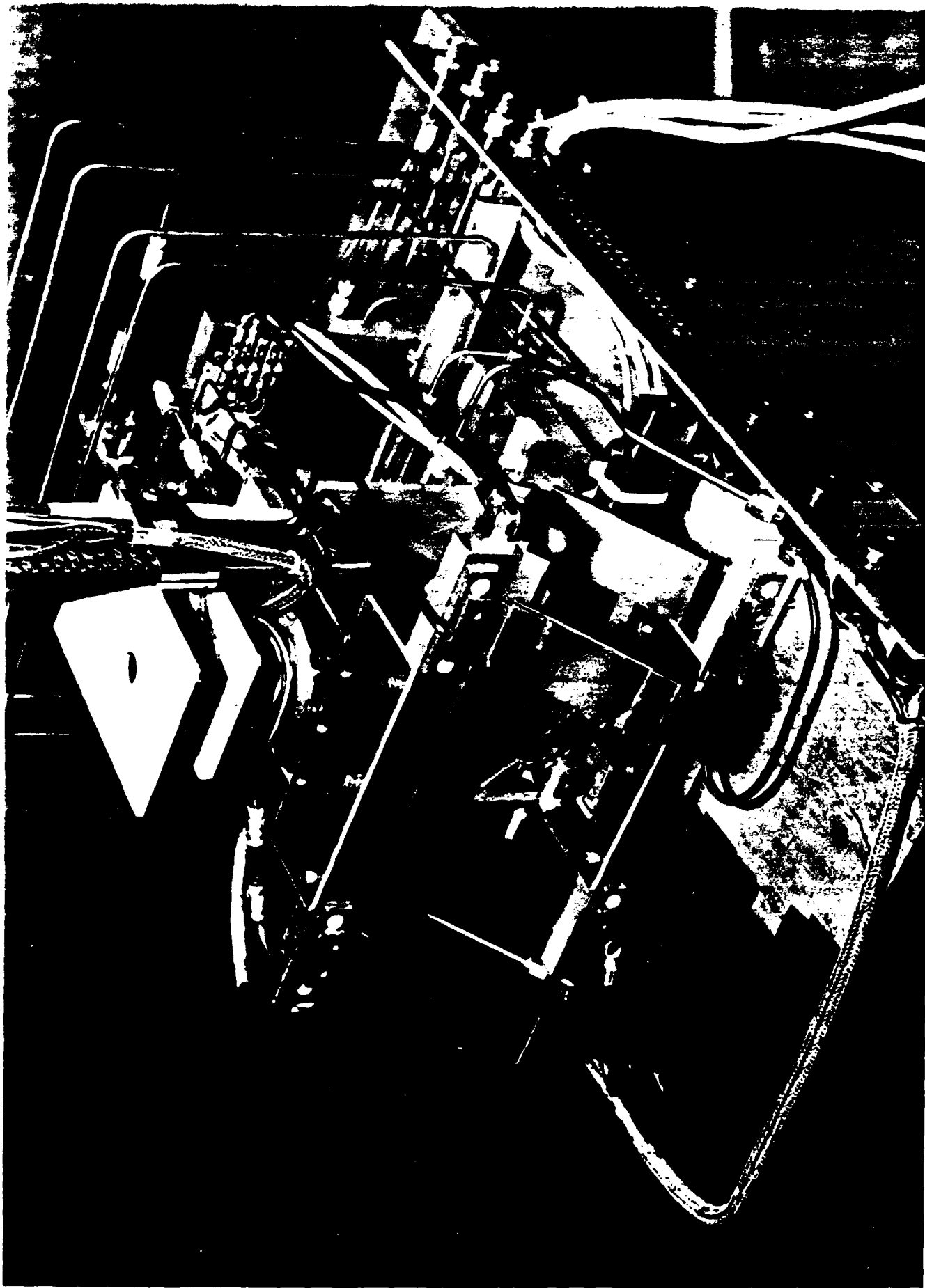


Fig. 18 - NASA LeRC Thrust Stand. Viewed from Electrical Connection Side.

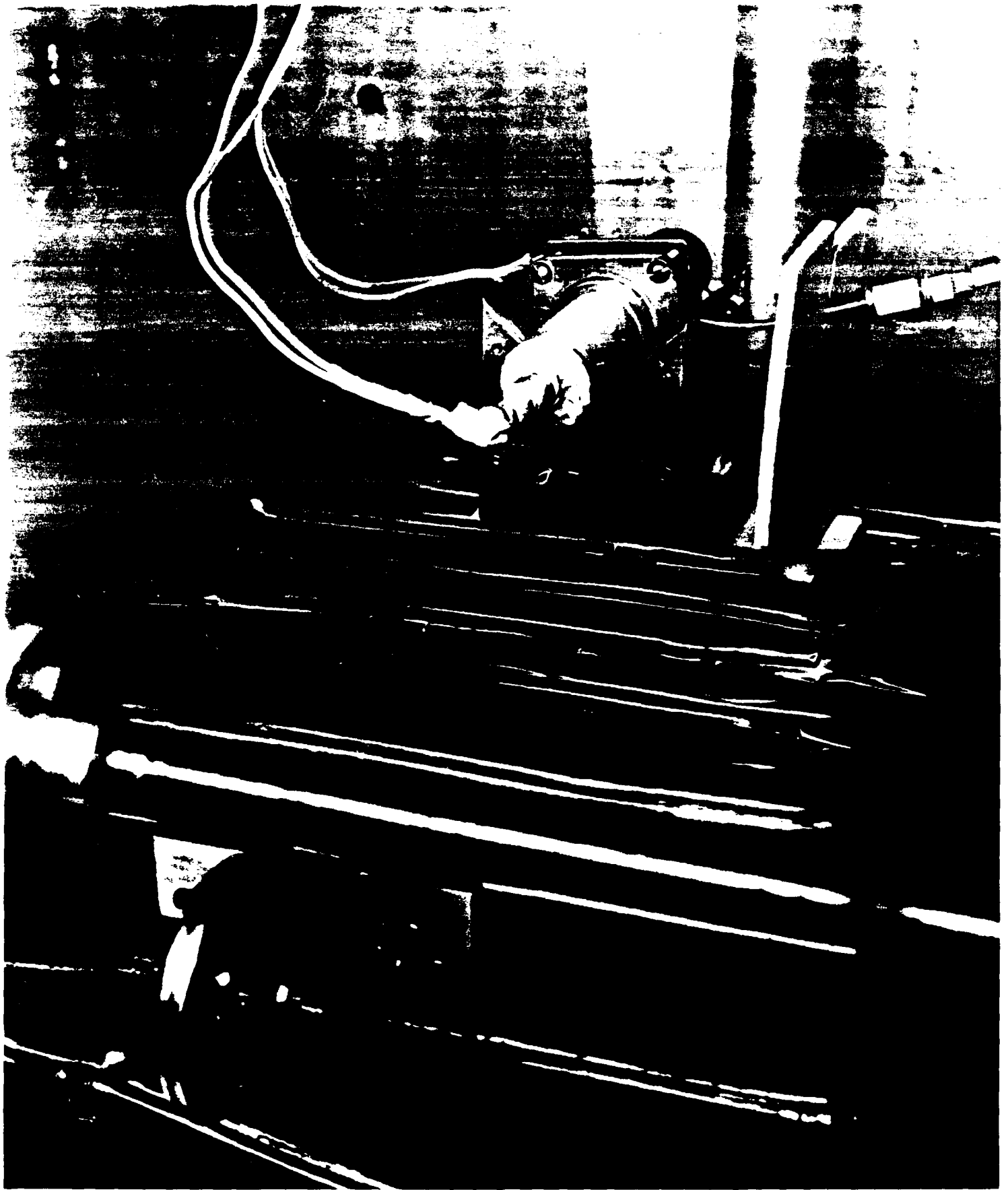


Fig. 19 - NASA LeRC Thrust Stand with Arcjet Mounted

TABLE 3 - THRUST STAND PARTS LIST

Part #	Description (Dimensions in Inches)	# Req.	Total
TS-			
01	Thruster mount support	1	1
02	Thruster top mounting plate	1	1
03	Bottom mount plate	1	1
04	Attachment plate	1	1
05	Top cooling coil plate	1	1
06	Cooling coil: 1/8 OD S.S.tubing	1	1
07	Bottom cooling coil plate	1	1
08	Thrust table	1	1
09	Flexures	8	16
10	Flexure holders	32	64
11	Flexure plates	2	2
12	Flexure clamps	16	16
13	Base plate	1	1
14	Upper tube support	1	1
15	Lower tube support	1	1
16	End plate	1	1
17	End plate cross member	1	1
18	Damper cross member	1	1
19	Damper bracket	1	1
20	Stop bracket	1	1
21	LVDT holder	1	1
22	LVDT core bracket	1	1
23	LVD	1	1
24	Damper forcing coil assembly	1	1
25	Water and Xe flex lines	5	5
26	Xe stand lines	3	3
27	Water and Xe connection lines	5	5
28	Male fittings: 1/8 SS	25	30
29	Female fittings: 1/8 SS	23	30
30	Connection strips	2	2
31	Leveling member	1	1
32	Bottom plate	1	1
33	Side plate	1	1
34	Flex bolts	2	2
35	Leveling actuator	1	1
36	Thermal couple wiring	-	-
37	Lead wiring	-	-
38	Ground shielding	-	-
39	Cu box top/ends	1	1
40	Cu box side - leads	1	1
41	Cu box side - other	1	1
42	Cu tubing: 1/4	-	-
43	Fittings: 1/4 male	2	2
44	Pulley	1	1
45	Pivots	2	2
46	Pulley brackets	2	2
47	Weights: 5 gm and 10 gm	5	5
48	Monofilament line	1	-
49	Take up drum	1	1

TABLE 3 - THRUST STAND PARTS LIST (CONCLUDED)

Part #	Description (Dimensions in Inches)	# Req.	Total
TS-			
50	Drum motor assembly	1	1
51	Drum position indicator assembly	1	1
52	Motor bracket	1	1
53	Connection strips: 15 power leads	3	3
54	Connection strips: 12 thermal couple leads	3	3
55	Connection strip LVTD	2	2
56	Connection strip damper	2	2
57	Connection strip leveler	2	2
58	Connection strip motor	2	2
59	Connection strip drum indicator	2	2
60	Wheels	4	4
61	Nuts, bolts, washers as required	-	-

## PLASMA DIAGNOSTICS PROBES

Two types of plasma probes which would be used in the diagnostics of the thruster's exhaust are: 1) an emissive probe, and 2) a guard ringed planer ion saturation probe. SeiTec anticipates that an existing AFAL x,y,z actuator would be made available for use with the various probes. SeiTec does not anticipate performing a detailed diagnostic study of the thruster exhaust beam, but rather a limited study to identify two fundamental things.

First, with the emissive probe, we would define the location of the plasma potential gradient which the expansion of the electron gas induces and which accelerated the ions of plasma. This, thus, defines physically where the plasma acceleration is occurring in the thruster's nozzles.

Second, with the planer ion saturation probe, we would define the degree to which the exhaust is columnated and directed in the desired downstream direction. Any deviation of the exhaust from the desired downstream direction is, of course, an inefficiency which has not been included in the, prior discussed, theoretical calculations. Therefore, these measurements can be important in reconciling the experimental measurements and the theoretical predictions.

Emmissive Probe - Figure 20 illustrates an emmissive probe design that has been successfully used for similar diagnostics of the exhaust of plasma thrusters, Ref. 4. If the thoriated tungsten filament of such a probe is heated to a sufficient temperature that further heating does not change its floating potential then the probe will be floating very near the plasma potential. Thus, with such probes one can map the plasma potential in the thruster's exhaust and, therefore, define the location of the ion acceleration process, as previously discussed.

Guard Ringed Planer Ion Saturation Probe - Figure 21 illustrates the design of a probe which has been successfully used by NASA LeRC in prior thruster exhaust beam tests, Ref. 5. By biasing such a probe into the ion saturation region, one obtains a reasonable estimate of the ion flux density as a function of position in the thruster exhaust. Note to very accurately measure the ion flux density, one would also need to measure the energy incident on the probe, Ref. 4. This additional information allows one to make a correction for the secondary electron emission from the probe face and to determine the ion energy, but this is beyond the scope required for the anticipated preliminary diagnostic investigation planned for this program.

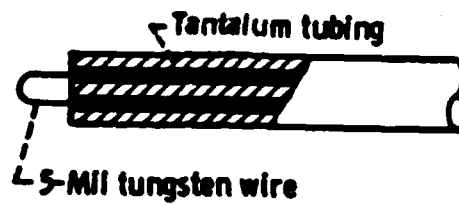


Fig. 20 - Emmissive Probe.

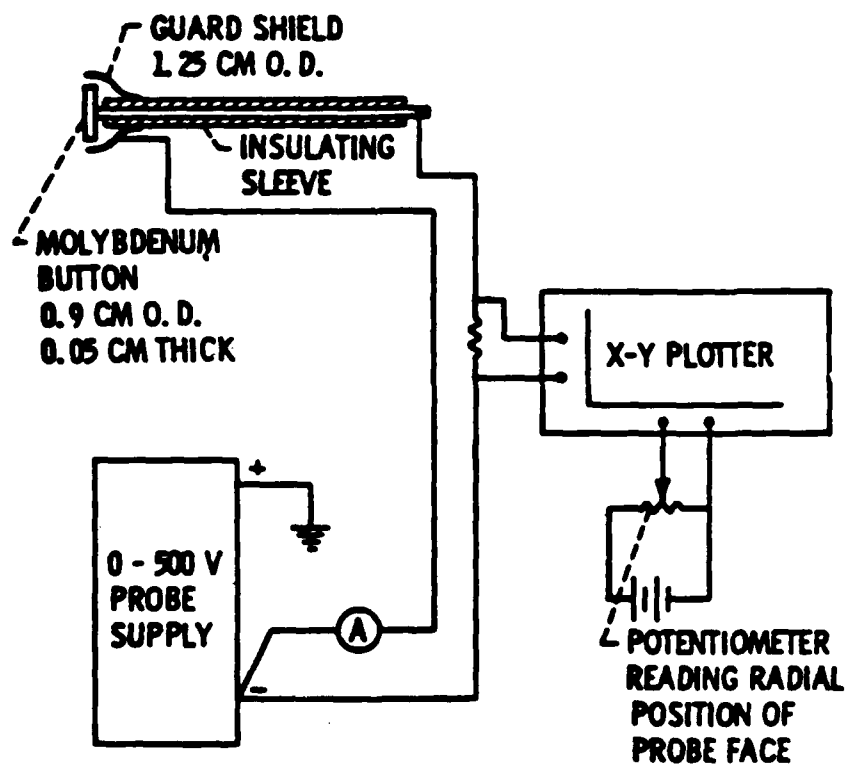


Fig. 21 - Guard Ringed Planer Ion Saturation Probe.



## EQUIPMENT PURCHASE

A significant amount of equipment is required to operate and test the subject thruster. Detailed lists, with cost for all the required equipment, are contained in Tables 4 and 5.

Figure 22 illustrates the various power supplies required to power the thruster and its coil systems. Also illustrated are the various planned voltage and current measurements. The main discharge power source of the thruster is divided into four modules which are nominally to be arranged in a series and parallel connection. This has been done to provide for greater flexibility in the range of voltage and current over which operation of the thruster could be explored by a rearrangement of the power supplies.

There are primary power supplies for both the shear and containment/nozzle coil systems. To provide for flexibility in the containment and nozzle field shapes, three additional trim power supplies have also been included. These would allow for exploring the effects on thruster performance of variations in the containment/nozzle field shapes.

The hollow cathode has both an operating power supply and a higher voltage, low current supply for cathode ignition.

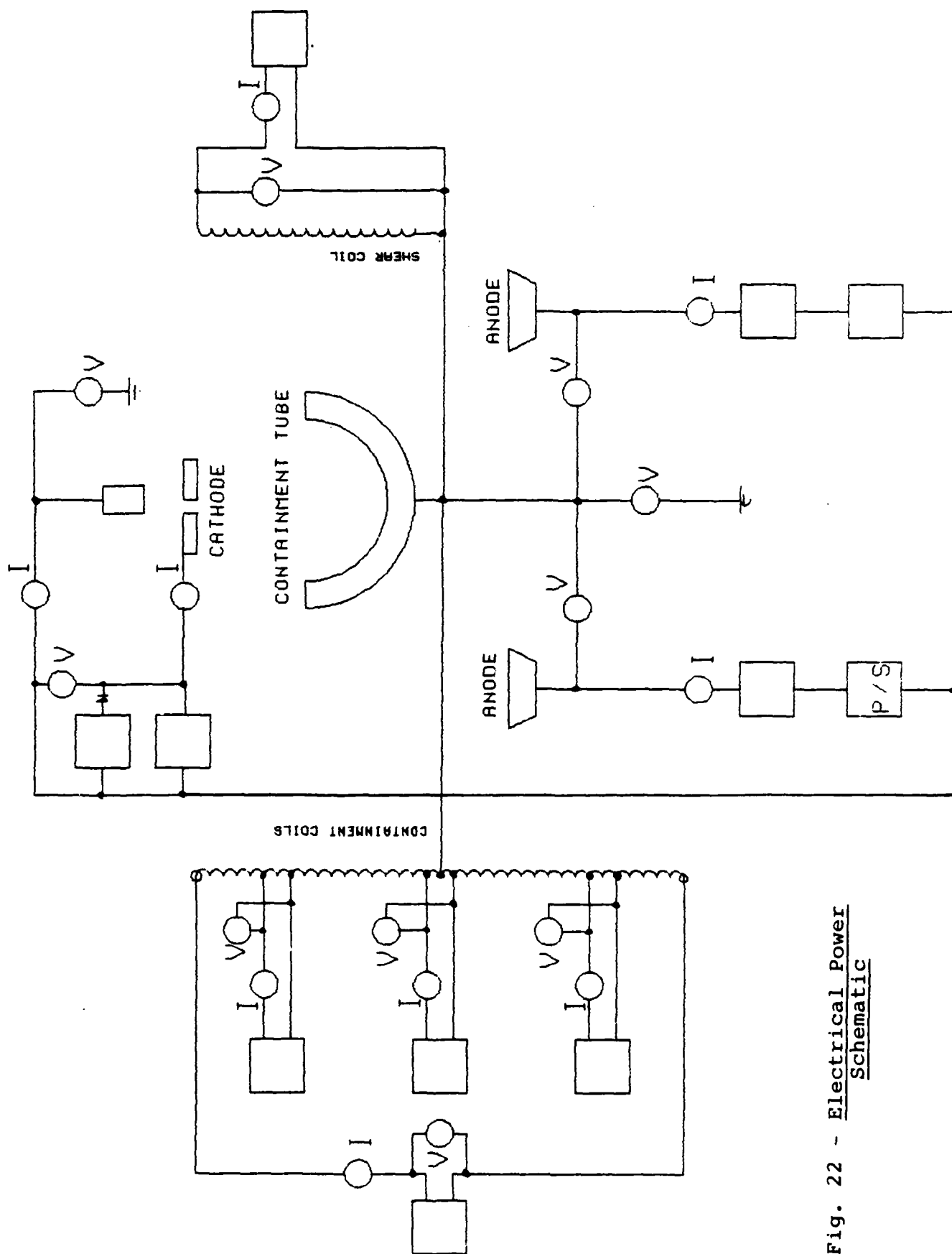


Fig. 22 - Electrical Power Schematic

It should be noted that most of the thruster current and voltage measurements and the thermocouples at various points on the thruster are required to be electrically floated. From past experience one would anticipate the cathode would float slightly below ground, the potential of the tank, and that the anode and coil systems would float substantially above ground. The electronic equipment required to convert these floating measurements to signals suitable for recording on the AFAL data system has been included in the required equipment.

Figure 23 illustrates the propellant system of the thruster. Propellant flow is independently controlled through four separate lines which feed the cathode, the two anodes, and the tank directly. The tank feed line is included to permit thruster performance to be measured as a function of tank background pressure. This is necessary in order to verify that the thrust is not a function of the tank pressure and therefore should be reliable. The cathode and anode propellant lines are at ground potential until after they have passed onto the thrust stand. Electrical isolation of the lines is provided on the thrust stand.

Also included in the Equipment Lists are the various other power supplies and equipment required for operation of the thrust stand, the diagnostic probes, for mapping of thruster fields, etc.

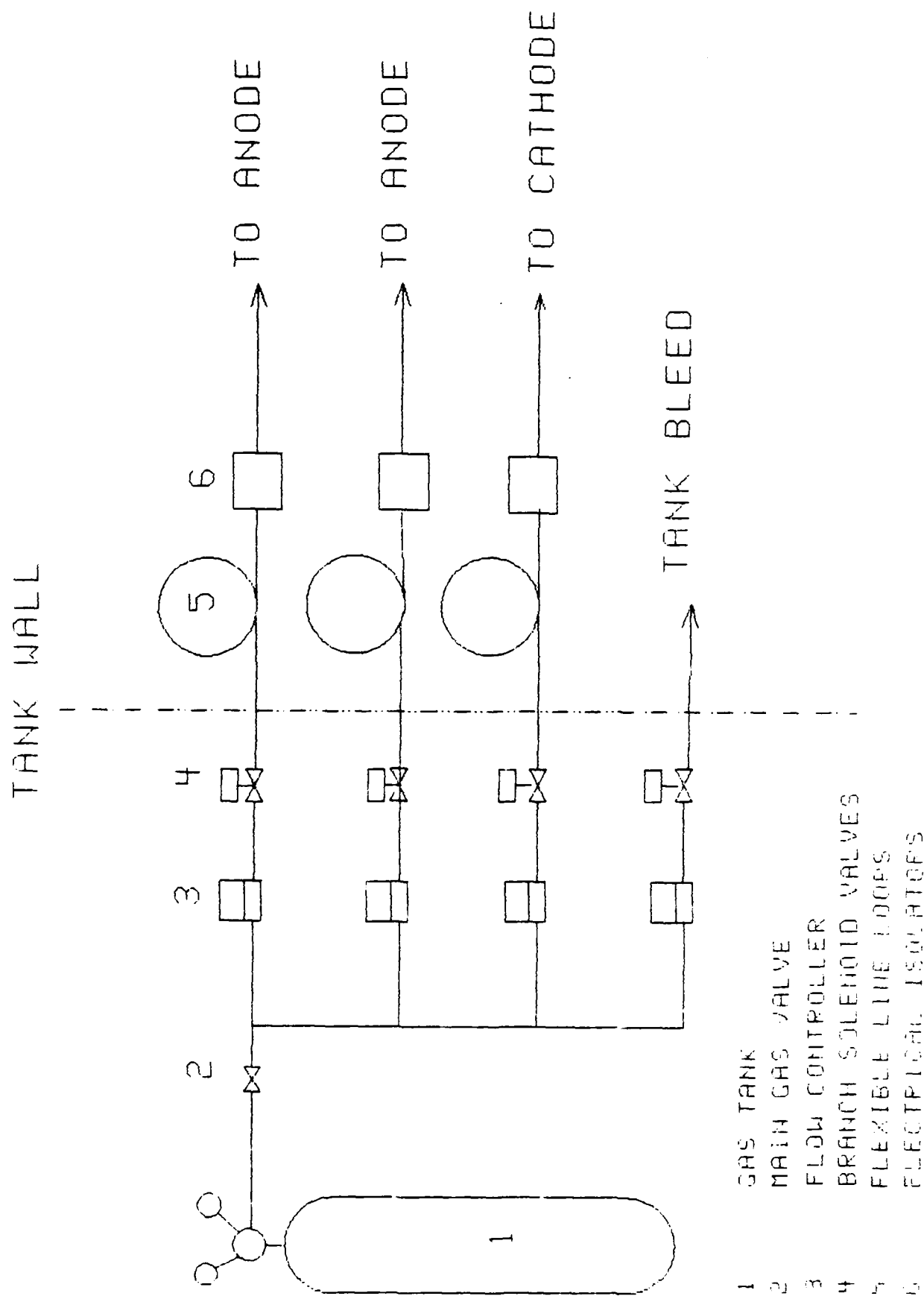


Fig. 23 - Gas System Schematic.

TABLE 4 - THRUSTER EQUIPMENT

ITEM	COST \$/EA.	QUANTITY
1. Power supply: Lambda LB706FM; 300V, 10A	3000.	4
2. Power supply containment and nozzle coils H-P 6268A,, 40V, 30A	900.	1
3. Power supply shear coils: EMC SCR 120-20-3011, 120V, 20A	1100.	1
4. Power supply trim: H-P 6281A; 7.5V, 5A	350.	3
5. Power supply cathode keeper: Trygon HR 60-5B, 60V, 5A	380.	1
6. Power supply cathode starter: Fluke 407D 550V, 0.3A	425.	2
7. Power supply solenoid valve: SOLA 05F1155, Type 28-24-280, 24V, 8A	270.	1
8. Panel meter : Newport Q9025, AVR3	375.	7
Panel meter : Newport Q90204VR3	270.	6
9. Interface isolating modules: Analog Devices 3B31	175.	9
3B47	250.	6
10. Isolation transformer: Topaz 91001-11; 1KVA	420.	4
11. Isolation transformer: Topaz 91415-11: 15KVA	3255.	1
12. Termination strips (6 terminals)	4.25.	8
13. Xenon gas 25 liters in steel tank	320.	1
14. Tank valve and regulation: Western LS-xxx	90.	1
15. Solenoid valve: Skinner V52DB1006 2-way	30.	1
16. Mass gas flow metering systems: Brooks 5850E	795.	4
17. Flow meter Electronic unit: Brooks 5896	520.	4
18. Solenoid valve: Skinner V52DB1006 2-way	30.	4
19. Electrical isolators - (in-tank)	150.	3
20. Cabinet and panels, AMCO	2000.	
21. Iron-constantan thermocouples materials 12T/c's	380.	12
Total Cost	\$42189.	

Note: Models cited were for costing only, actual model would be cited or equivalent.

TABLE 5 - THRUST STAND AND DIAGNOSTICS EQUIPMENT

ITEM	COST \$/EA.	QUANTITY
1. LVDT sensor: Schaevitz .250 MHR	158.	1
2. LVDT controller and meter: Schaevitz DTR-451	340.	1
3. Electro - mechanical VIB damper (to make)	600.	1
4. Stepping motor controller: Superior electric ST101A	788.	1
5. Stepper motor: M091 Superior Electric	147.	1
Superior Elect Drop Resistor	20.	
6. Weight Level Indicator: - Potentometer: Duncon	147.	1
P/N 3203RIK.1	69.	2
Weight Level Indicator: PWR. SUP. Trygon		
T50-750 50V, .75A	225.	1
7. Gaussmeter and probes: Bell 610	2400.	1
8. Pyrometer: WAHL HSM - 671	3035.	1
9. Vacuum micron gage, control and gage	565.	1
10. Vacuum high vacuum gage controller and gage: Varian 843	970.	1
11. 2 Pen X-Y Plotter	4500.	1
12. Probe AC heater power supply: Superior Electric No. 21 Powerstat; XFMR step down	55.	1
13. Oscilloscope and accessories: Gould OS 300 LP	760.	1
14. Linear Actuator: Warner Electric	105.	1
15. Linear Actuator Control: Warner Electric MCS-2005	100.	1
16. Current Transducer: American Aerospace controls series 903B 5AMP	300.	3
17. Current xducer: American Aero Ser. 950 10A	360.	1
18. Current xducer: American Aero Ser. 950 20A	360.	2
19. Current xducer: American Aero Ser. 950 30A	360.	1
20. Thermocouple wire & Acces. set: Omega	380.	1
21. Thermocouples, set of 12	200.	1
22. Wt. lift drive: Bodine Mod. 725	96.	1
23. Ion Probe Power Supply: HP 6521A	1500.	1
Total Cost		\$19624.

Note: 1) xduces = Transducer  
 2) Models cited are for costing only, actual model would be cited or equivalent.

## THRUSTER OPERATING PROCEDURE

Testing of the thruster would follow the following procedure:

- 1) After installation of the thruster and thrust stand in the test facility, cooling water to the thrust stand would be initiated and a check for leaks made.
- 2) The thrust stand would be turned-on and the level of the thrust stand would be adjusted so that its LVDT displacement transducer is approximately in the middle of its operating range as the calibration weights are added and removed.
- 3) The facility would be closed and pumped down to less than  $10^{-5}$  torr, and the direction of thrust stand drift, due to facility movement during pump-down, will be recorded.
- 4) After pump down, the thrust stand would be remotely releveled to return the LVDT transducer output to its prepump down position, and the thrust stand would be recalibrated.
- 5) Thruster operation is then initiated by starting the downstream hollow cathode. This is accomplished by:
  - a) Turning on a propellant flow to the cathode equal to approximately one half the design anode flow. Based on NASA LeRC data, this should reduce the required breakdown voltage to approximately 500 volts.
  - b) The cathode keeper and starter power supplies are then turned-on.
  - c) After the cathode is ignited, the cathode flow is reduced

to its operating level; a few percent of the desired anode flow.

6) The magnetic fields of the thruster are then turned-on to their desired strength, and monitoring of thruster temperatures is initiated.

7) The desired propellant flow is next introduced into each anode.

8) The main discharge power supply is then started and the voltage increased until the desired operating current is achieved. As the current is increased, equal anode currents should be maintained by fine adjustment of the anode flows; increasing or decreasing flows should respectively increase or decrease current. Also, as the main discharge current is increased, cathode flow and keeper current can be adjusted to provide some control of the main discharge current at a set voltage. Increasing or decreasing either cathode flow or keeper current should respectively increase or decrease the main discharge current.

9) Periodically during testing, and at its completion, the thrust stand calibration weights should be lowered and raised to insure there is no drift or change in calibration of the stand.

10) For desired operating conditions, the probe accumulator will be used to traverse the diagnostics probes horizontally through the thruster exhaust beam at a number of heights from the thruster center plane and distances from the thruster exit plane.

11) Shut down of the thruster is accomplished by first turning-off the main discharge power supply and then the cathode starter and keeper supplies; the magnetic field power supplies can



then be turned-off and the propellant flows shut-off.

12) No problem is anticipated from shutting-off the cooling water to the thrust stand while the facility is still evacuated, if the facility does not have an operating cryopanel; but the safest procedure is to maintain cooling water flow until the facility is bled-up to atmospheric pressure. However, the facility must be maintained at low pressure until the temperature of the thruster is at a safe level for avoiding damage due to oxidation.

#### REFERENCES

1. Seikel, G.R., and Franks, C.V., "Completely Magnetically Contained Electrothermal Thrusters," AIAA-85-2053, 1985.
2. Connolly, D.J., and Bishop, A.R., and Seikel, G.R., "Tests of Permanent Magnet Superconducting Magnet MPD Thrusters," AIAA-71-696, 1971.
3. Johansen, A.E., and Palmer, R.W., "Lightweight Magnets for MPD Arcs," AIAA-67-686, 1967.
4. Bowditch, D.N., "Investigation of the Discharge and Exhaust Beam of a Small Arc Plasma Thruster," AIAA-66-195, 1966.
5. Burkhart, J.A., and Seikel, G.R., "Feasibility Studies on an Auxiliary Propulsion System using MPD Thrusters," AIAA-71-695, 1971.
6. Connolly, D.J., and Sovie, R.J., "The Effect of Background Pressure and Magnetic Field Shape on MPD Thruster Performance," AIAA-69-243, 1969.
7. Walker, E.L., and Seikel, G.R., Axisymmetric Expansion of a Plasma in a Magnetic Nozzle Including Thermal Conduction, NASA TN D-6154, NASA LeRC, Cleveland, OH, 1971.

## APPENDIX A - THRUSTER PERFORMANCE ANALYSIS

As discussed by Seikel and Franks in Ref. A-1, the performance of any DC arc thruster can be evaluated on the basis of a power balance which considers the useful thrust power and all of the various thruster power losses. For a thruster producing a fully ionized exhaust and operating with a specified propellant, mass flow, power level, and voltage, a power balance can be written. If we define

$$\text{Discharge voltage in V: } V \quad \text{Eq. A-1a}$$

$$\text{Discharge current in A: } I \quad \text{Eq. A-1b}$$

$$\text{Power input in W: } P = VI \quad \text{Eq. A-1c}$$

$$\text{Thrust in N: } T \quad \text{Eq. A-1d}$$

$$\text{Mass flow in kg/s: } \dot{m} \quad \text{Eq. A-1e}$$

$$\text{Efficiency: } \eta = T^2 / 2\dot{m}P \quad \text{Eq. A-1f}$$

$$\text{Specific impulse in s: } I_{sp} = T / g\dot{m} \quad \text{Eq. A-1g}$$

where  $g$  is  $9.806\text{m/s}^2$ .

The useful power is the thrust power in W:

$$P_T = T^2 / 2\dot{m} = g^2 \dot{m} I_{sp}^2 / 2 \quad \text{Eq. A-2}$$

The major unavoidable power losses are those associated with conducting current to the anode, emitting current from the

cathode, ionizing the propellant atoms in the plasma volume, and diffusion and recombinations of plasma on the thruster's surfaces. These power losses in watts are:

$$\text{Anode power: } P_A = (2kT_e/e + \phi_A)I \quad \text{Eq. A-3}$$

$$\text{Cathode power: } P_C = \phi_C I + P_{RC} = \phi_{Ce} I \quad \text{Eq. A-4}$$

$$\text{Ionization power: } P_I = \phi_e \dot{m}_e / m_i \quad \text{Eq. A-5}$$

Backplate power (diffusion only,  $T_i/T_e \approx 0$ ):

$$P_B = 0.6F\{\phi_e + [2.5 + 0.5 \ln(m_i/2\pi m_e)]kT_e/e\} \dot{m}_e / m_i \quad \text{Eq. A-6}$$

where  $F$  is a factor between 0 & 1

$P_{RC}$  is the cathode radiation, W

$T_e$  and  $T_i$  are the electron and ion temperatures, K

$e$  is the abs. value of an electron charge,  $1.6021 \times 10^{-19}$  C

$k$  is Boltzmann's constant,  $1.38054 \times 10^{-23}$  J/K

$m_{e,i}$  are electron and propellant ion mass, kg

$\phi_{A,C,Ce}$  are the anode, cathode, and effective cathode work functions, V

$\phi_e$  is effective volume ionization cost, V

The thruster efficiency,  $\eta$ , is determined, using Eqs. A-2 - A-6, as the ratio of useful power to total power, which is equal to the useful power plus power losses. Thus

$$\eta = \frac{1 - (\phi_A + \phi_{Ce} + 2kT_e/e)/V}{1 + \left[ \phi_e (1 + 0.6F) + F \left[ 1.5 + 0.3 \ln \frac{m_i}{2\pi m_e} \right] \frac{kT_e}{e} \right] \frac{2e}{m_i g^2 I_{sp}^2}} \quad \text{Eq. A-7}$$

And also from Eqs. A-1f and A-1g

$$\eta = \frac{\dot{m}}{2P} g^2 I_{sp}^2$$

Eq. A-8

As discussed below, the simultaneous solution of Eqs. A-7 and A-8 defines the thruster operating point.

Note only diffusion to a thruster's insulating backplate, for the case of cold ions, is considered. For thrusters with an applied magnetic field, this is the only thruster component normal to the magnetic field. Therefore, it is the principle recipient of the diffusing plasma. To account for either complete or partial magnetic containment of the plasma, a factor (F), has been included in this backplate loss; this factor can be parametrically varied from 0 to 1. Note, if there is either a population of high energy electrons on top of the Maxwellian distribution or if the applied magnetic field is shaped to accelerate plasma toward the backplate of the thruster, the backplate loss could be even higher than that due to only diffusion.

For a typical thruster with a molybdenum anode and a hot thoriated tungsten cathode, the sum of the anode work function plus effective cathode work function in Eq. A-7 can be well approximated as 10 volts. With this assumption, note that the efficiency given by Eq. A-7 would become zero at an electron temperature equal to one half the applied voltage minus 10; all the power would be consumed in anode and cathode losses. Thus,

the magnitude of the applied voltage determines an upper bound on electron temperature.

The volume ion production costs in Eq. A-7 can be evaluated using the approximate general theory of Dugan and Sovie, Ref. A-2. Their theory takes into account the competition between ionizing and exciting collisions of electrons with propellant atoms. Such an approach is strictly valid only for low density, so called tenuous plasmas. However, a more detailed study of ionizing helium showed that inclusion of collisions with metastable states only slightly affected (increased) the cost of producing ions. Results are illustrated for argon and xenon in Fig. A-1. Since the cost of producing ions becomes unbounded as the electron temperature approaches zero, the efficiency given in Eq. A-7 becomes zero at zero electron temperature. Note, in a DC thruster one might expect to have a population of higher energy electrons (directly emitted from the cathode) in addition to the Maxwellian electron distribution. Dugan and Sovie have, however, shown that the primary interaction in a volume of such higher energy electrons is to heat by instability the Maxwellian electron distribution and not to directly produce ions.

With the above assumptions, Eq. A-7 can be used to determine how the efficiency of a thruster, operating with a given discharge voltage, varies as a function of specific impulse if one can

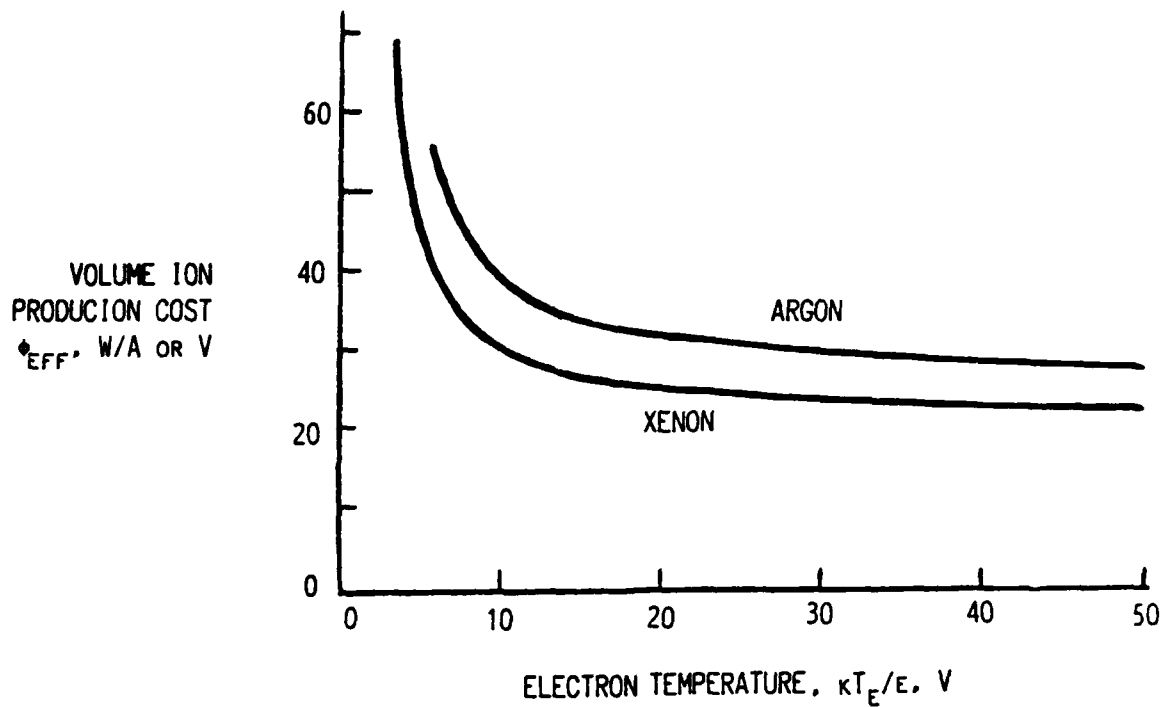


Fig. A-1 - Volume Ion Production Cost.

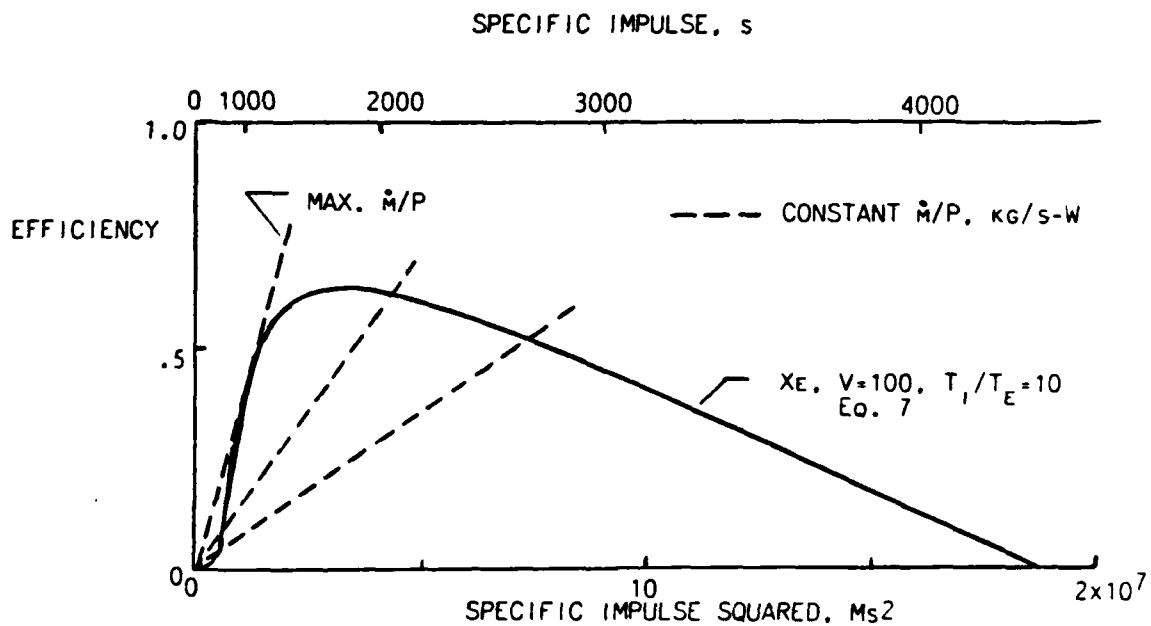


Fig. A-2 - Theoretical Electrothermal Applied - Field MPD Thruster Performance. Adiabatic Expansion, No Backplate Losses.

relate electron temperature and the specific impulse. The specific operating point of a thruster operating with a specified mass flow to power ratio can then be determined by the innersection of Eqs. A-7 and A-8, as illustrated in Fig. A-2. Note, generally, the high specific impulse solution is the one of interest. In this example, the expansion of the gases is assumed to be adiabatic and the ion to electron temperature ratio is assumed to be 10. For an adiabatic expansion, the temperatures and specific impulse are related by:

$$k(T_e + T_i)/e = 0.2g^2 I_{sp}^2 \quad \text{Eq. A-9}$$

It is interesting to also note from Fig. A-2 that there is a maximum mass flow to power ratio at which the thruster can operate.

Walker and Seikel, Ref. A-3 have examined analytically the alternative type of expansion process found in the low power MPD arc thrusters, specifically, the expansion of a fully ionized plasma containing hot electrons and cold ions. They assumed a magnetic nozzle produced by a Helmholtz set of coils, Fig. A-3. The analysis is restricted to near the axis of symmetry, and the effects of thermal conduction, which can be very important are included. As indicated in Fig. A-3, a large increase in final velocity over that which would be obtained in an adiabatic expansion is possible. The set of equations solved include the

electron and ion continuity and momentum equations, Maxwell's equations, and the electron energy equation. No asymptotic solutions to this nonlinear set of equations for large values of distance were found using classical values of the conductivity for the plasma. As a result, and due to the fact that in experiments major fluctuations are present, an assumption was introduced that the electron collision time could be replaced by an effective time. In particular, the assumption was made that the effective Hall parameter was a constant throughout the flow. Such an assumption assumes a saturation of this parameter which has been experimentally observed in MHD generators and plasma thrusters. Chubb and Seikel (Ref. A-4), for example, found that the effective Hall parameter in a Hall current ion thruster saturated at a value of three. This value is also used for the calculations herein. With this additional assumption, the solutions to the plasma expansion shown in Fig. A-3 were obtained. The ordinate is the ratio of final ion energy to initial electron energy, that is, the final ion energy at the end of the expansion divided by the random energy the electrons had before the expansion started. This is plotted against the sonic point location. The sonic point location is relative to the downstream coil in the Helmholtz set. Zero is at the plane of the coil and distance is given in coil radii. The parameter in the analysis is a nondimensional parameter best thought of as a nondimensional magnetic field. As this parameter becomes large, the solutions approach the adiabatic limit.



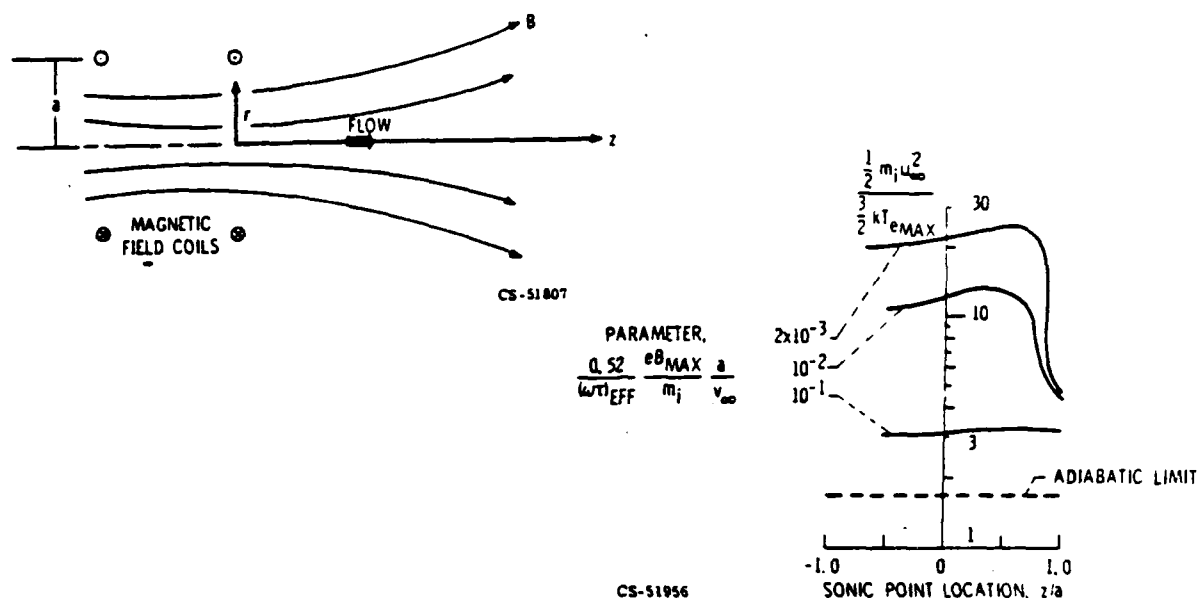


Fig A-3 - Expansion of a Cold-Ion, Hot-Electron Plasma in a Magnetic Nozzle.

These solutions illustrate a couple of points. First, the magnitude of the ratio of final ion energy to initial electron energy can be much larger than that of an adiabatic expansion. This illustrates how important thermal conduction can be in such a process. Second, the solutions are quite sensitive to the location of the sonic point in the flow, and therefore, to the divergence of the magnetic nozzle.

The results of Fig. A-3 can be used in Eq. A-7 to complete the power balance for a low power MPD arc thruster. Fig. A-4 compares the experimental data of the thruster of Ref. A-5 with the results of such an analysis. Three analytical curves are

shown. The first is for a thruster with an optimum shaped magnetic nozzle and no backplate losses. The other two are both for thrusters with much too rapidly expanding magnetic nozzles. One assumes no backplate loss, and the other assumes a maximum diffusion backplate loss.

The pole pieces used in this thruster did produce a rapidly expanding magnetic field. This was done in an attempt to improve containment of the plasma from the backplate. Comparison of the data and analysis would appear to indicate that although some containment is obtained by such a mirror field, the backplate loss is still approximately half of the maximum value for diffusion.

These results indicate that the reason this thruster had higher performance than previous thrusters is solely due to its higher operating voltage. If complete magnetic containment of the plasma is utilized and the shape of the magnetic nozzle optimized, these results further indicate that thrusters with performance between 60 and 80% should be feasible in the 2500 to 3500 second specific impulse range.

Figure A-5 indicates the performance potential for the high power, high magnetic field thrusters in which ion temperature is important and the expansion should be adiabatic. Shown are the anticipated performance for completely magnetically contained

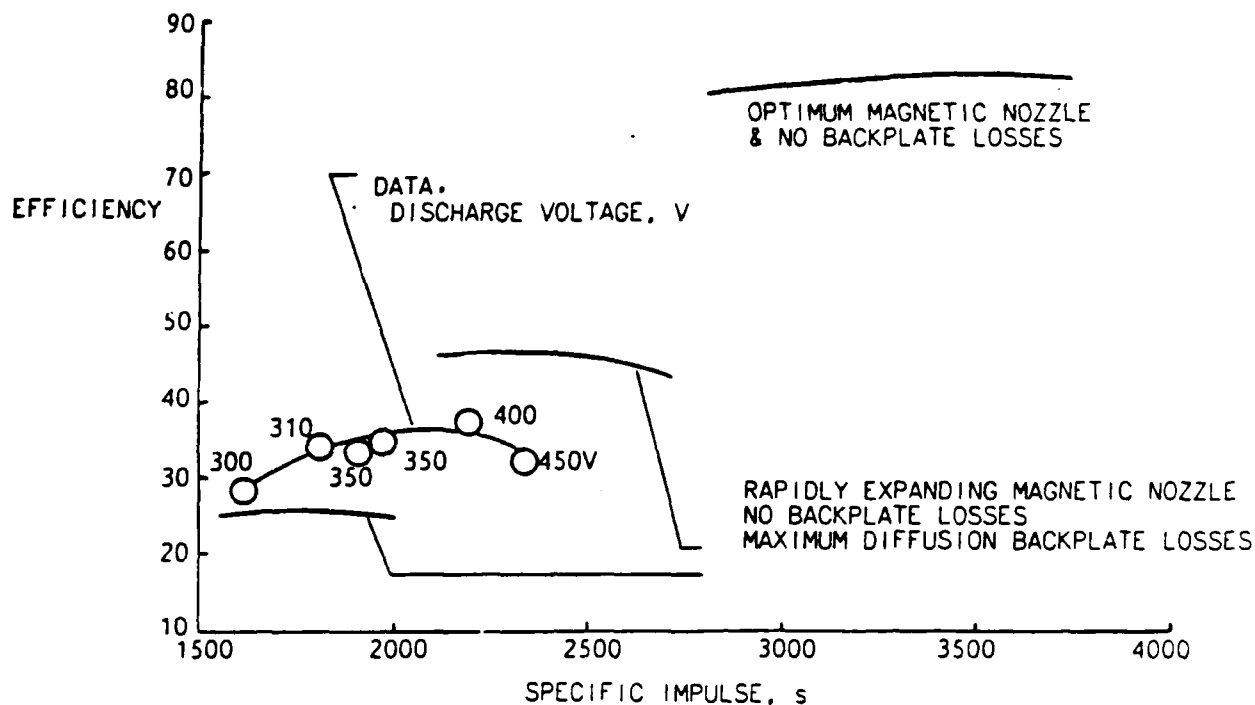


Fig. A-4 - Comparison of Experimental and Theoretical Performance of 0.5 kW, 0.03T Applied-Field MPD Thruster.

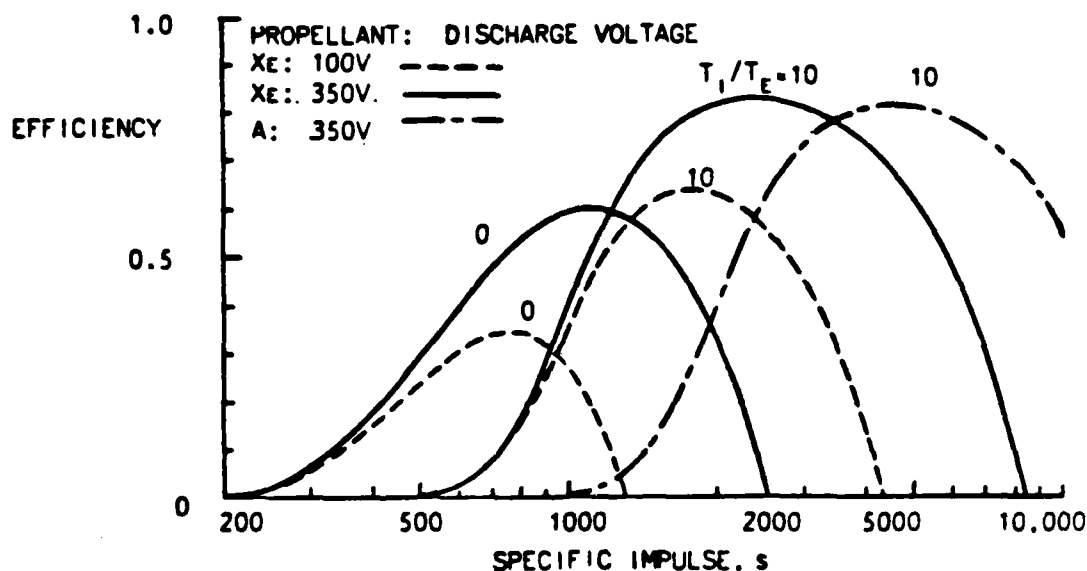


Fig. A-5 - Theoretical Performance of High-Power High-Magnetic Field Thrusters.

xenon thrusters operating at two different voltages and ratios of ion to electron temperature. Also indicated is the expected performance of an equivalent argon thruster. As indicated these thrusters should also have the potential of approaching 80% efficiency if high ratios of ion to electron temperature are obtained in the discharge.

#### REFERENCES APPENDIX A

A-1. Seikel, G. R., and Franks, C. V., "Completely Magnetically Contained Electrothermal Thrusters," AIAA paper number AIAA-85-2053, 1985.

A-2. Dugan, J. V. Jr, and Sovie, R. J., Volume Ion Production Costs in Tenuous Plasmas: A General Atom Theory and Detailed Results for helium, Argon, And Cesium, NASA TN D - 4150, NASA LeRC, Cleveland, OH, 1967.

A-3. Walker, E. L., and Seikel, G. R., Axisymmetric Expansion of a Plasma in a Magnetic Nozzle Including Thermal Conduction, NASA TN D - 6154, NASA LeRC, Cleveland, OH, 1971.

A-4. Chubb, D. L., and Seikel, G. R., Basic Studies of Low Density Hall Current Ion Accelerator, NASA TN D - 3250, NASA LeRC, Cleveland, OH, 1966.

A-5. Burkhardt, J. A., "Performance of a Modified Downstream - Cathode MPD Thruster." J. of Spacecraft and Rockets. Vol. 10, No. 1, 1973, pp. 86 - 88.

## APPENDIX B - GENERAL MAGNETIC FIELD CONSIDERATIONS

### B-1 - MAGNETIC FIELD OF A TOROIDAL COIL

From Ampere's circuital law (Ref. B-1, p. 160)

$$\oint_C \mathbf{B} \cdot d\mathbf{l} = \mu_0 \int_S \mathbf{j} \cdot \mathbf{n} da \quad \text{Eq. B-1}$$

one can simply show that the magnetic field inside of a toroidal coil, Fig. B-1, varies inversely with the value of the major radius, R:

$$\oint_C \mathbf{B} \cdot d\mathbf{l} = B_z 2 \pi R \quad \text{Eq. B-2}$$

$$\int_S \mathbf{j} \cdot \mathbf{n} da = I N \quad \text{Eq. B-3}$$

where  $IN$  is the ampere turns of the toroidal solenoid. Therefore

$$B_z = \mu_0 I N / 2 \pi R \quad \text{Eq. B-4}$$

Where  $\mu_0$  is the magnetic permeability of free space,  $4\pi \times 10^{-7}$  H/m.

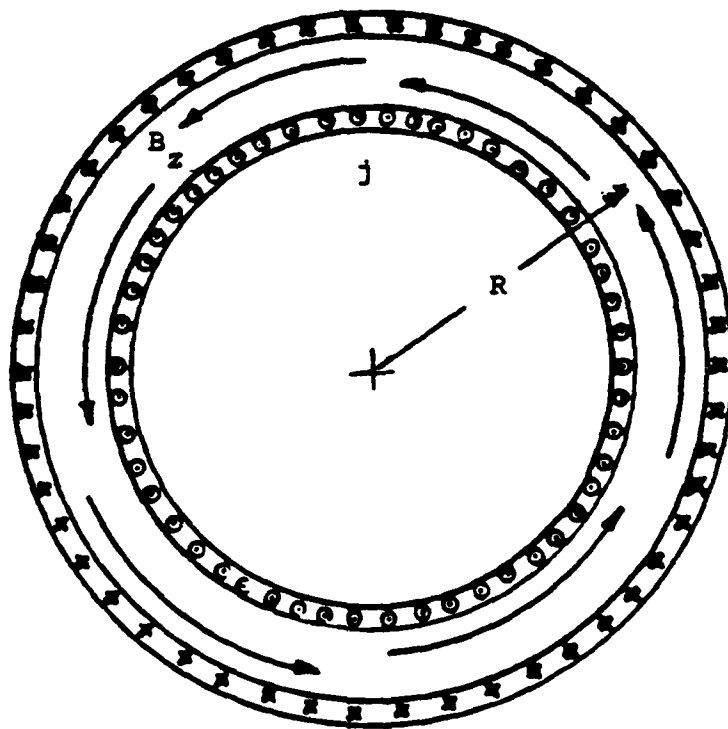


Fig. B-1 - Toroidal Solenoid.

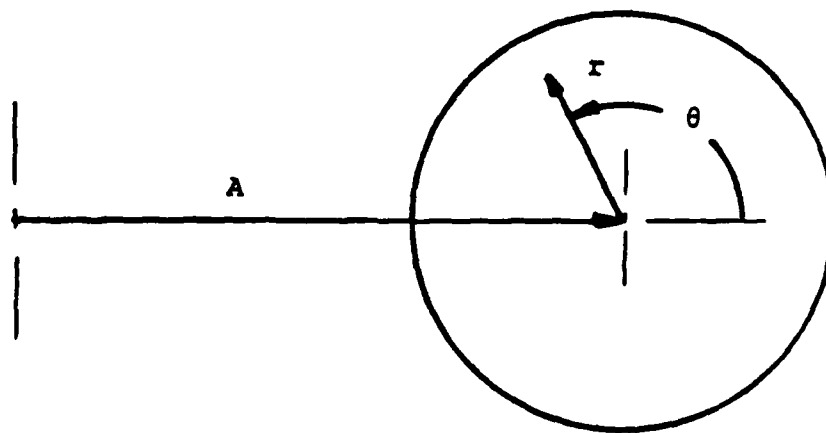


Fig. B-2 - Crosssection of Toroidal Solenoid.

If one defines a coordinate system inside the torrus as illustrated in Fig. B-2, then Eq. B-4 becomes

$$B_z = \mu_0 I N / [ 2 \pi ( A + r \cos\theta ) ] \quad \text{Eq. B-5}$$

It is well known that charged particles (electrons or ions) cyclotroning in a magnetic field with a transverse gradient of the field strength will experience a drift (Ref. B-2). This physically results from the fact that the cyclotron radius of a particle will be smaller in the high field than in the lower field. As illustrated in Fig. B-3 particles of opposite sign cyclotron and therefore drift in opposite directions.

Since a plasma must remain charge neutral, these opposite direction drifts of electrons and ions induce an electric field, as illustrated in Fig. B-4, which in turn results in a drift of both electrons and ions in the  $\mathbf{E} \times \mathbf{B}$  direction. This results in transporting the plasma towards the lower strength magnetic field or in a toroidal field to the outside major radius of the torrus.

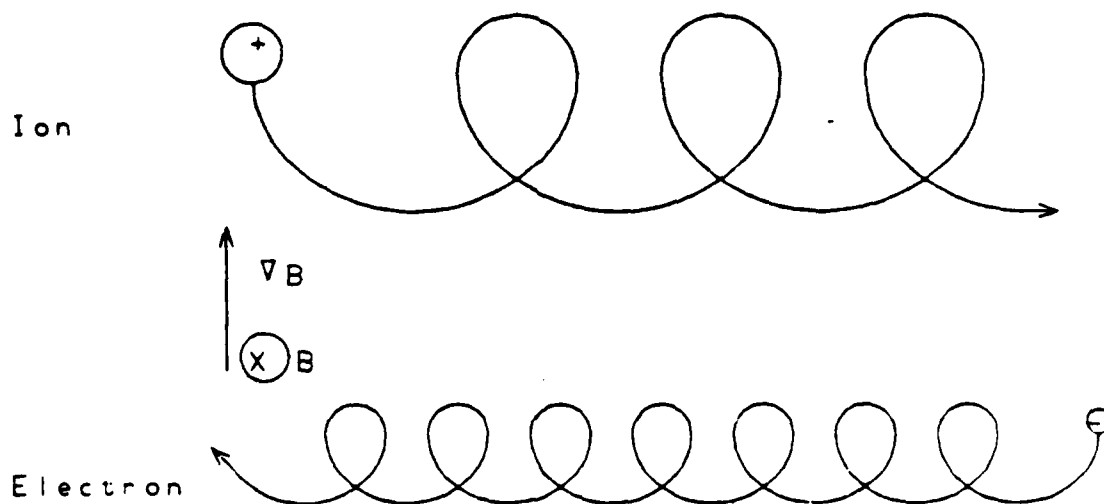


Fig. B-3 - Drift Produced by Magnetic Field Gradient.

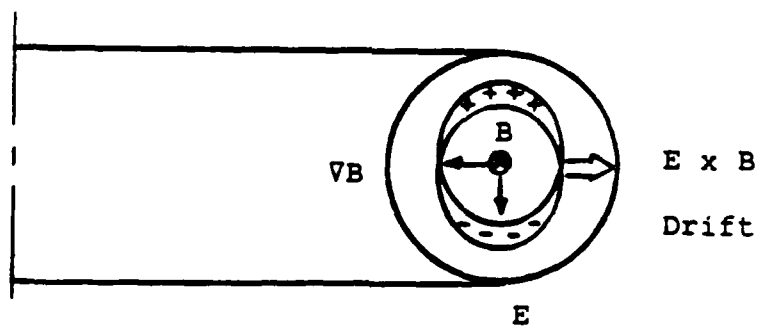


Fig. B-4 - Drift of Plasma in a Simple Toroidal Magnetic Containment Field.



## B-2 - MAGNETIC FIELD OF HELICAL COILS WITH OPPOSING CURRENT FLOW

The basic configuration of a set of helical wound coils with opposing currents,  $I_s$ , in  $2N$  conductors where  $N = 3$  and the axial pitch of the conductors  $\lambda = 2 \pi N / h$  is illustrated in Fig. B-5.

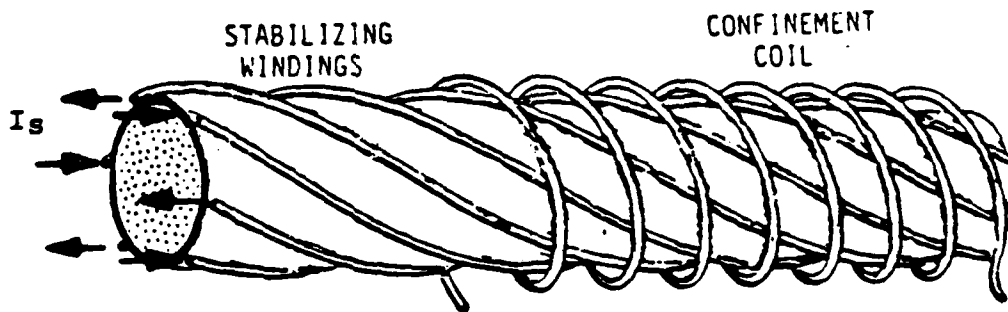


Fig. B-5 - Configuration of Helical Coils.

As indicated in Ref. B-3. (p. 431), the magnetic fields of such coils is well approximated by

$$B_r = C r^{N-1} \sin( N \theta - h z ) \quad \text{Eq. B-6a}$$

$$B_\theta = C r^{N-1} \cos( N \theta - h z ) \quad \text{Eq. B-6b}$$

where C is a constant of the coil geometry and magnitude of the current  $I_s$ .

Rose and Clark, Ref. B-3, further indicate that the angle,  $\phi$ , thru which a magnetic line twists about the magnetic axis in a distance, z, equal to one helical coil pitch,  $\lambda$ , is

$$\phi(z=\lambda) = \left[ \pi N C^2 r^{2N-4} / h^2 B_{z0}^2 \right] \left[ 2(N-1) + h^2 r^2 \right] \quad \text{Eq. B-7}$$

where the term  $h^2 r^2$  can be ignored except if  $N = 1$ .  $B_{z0}$  is the magnitude of the axial imposed magnetic flux density.

By inspection of Eq. B-7, one notes that  $\phi$  is not a function of r unless  $N > 2$ . For  $N = 3$ ,  $\phi$  increases with r and the field is said to have "shear". Magnetic shear is necessary to contain a plasma, that is to have a plasma pressure that decreases with radius (as will be discussed in Appendix C-1).

Since  $N = 3$  is the simplest helical coil configuration which

will provide magnetic shear, it will be the only case considered herein.

For  $N = 3$ , Eqs. B-6 and B-7 become

$$B_r = C r^2 \sin(3 \theta - 6 \pi z / \lambda) \quad \text{Eq. B-8a}$$

$$B_\theta = C r^2 \cos(3 \theta - 6 \pi z / \lambda) \quad \text{Eq. B-8b}$$

$$\phi = C^2 r^2 \lambda z / (3 \pi B_{z0}^2) \quad \text{Eq. B-8c}$$

where by superposition of the fields of six such wires, one can show that:

$$C \sim 3 \mu_0 I_s / (\pi a^3) \quad \text{Eq. B-9}$$

### B-3. COMPARISON OF EXIT FIELDS OF A LONG SOLENOID AND A HELMHOLTZ COIL

From Ref. B-1 ( p. 153 ), one obtains that the magnetic field on the axis of a semi-infinite solenoid of radius  $a$  is

$$B_z(z) = (\mu_0 NI/2L)(1 + \cos \alpha) \quad \text{Eq. B-10}$$

where

$$\cos \alpha = -z/(z^2 + a^2)^{1/2} = -\xi/(1 + \xi^2)^{1/2} \quad \text{Eq. B-11}$$

if  $\xi = z/a$  and  $z$  is measured from the solenoid exit plane.  
Therefore

$$B_z = (\mu_0 NI/2L)[1 - \xi/(1 + \xi^2)^{1/2}] \quad \text{Eq. B-12}$$

and

$$(dB_z/d\xi)/B_z = -1/[(1 + \xi^2)^{3/2} - \xi(1 + \xi^2)] \quad \text{Eq. B-13}$$

Thus for  $\xi = 0$

$$(dB_z/d\xi)/B_z = -1 \quad \text{Eq. B-14}$$

From Ref. B-1 (p. 156), one obtains that the magnetic field on the axis of a circular coil of radius  $a$  and current  $NI$  is

$$B_z(z) = (\mu_0 NI/2)[a^2/(a^2 + z^2)^{3/2}] \quad \text{Eq. B-15}$$

Therefore, the magnetic field on the axis of a Helmholtz coil, two coils with identical currents ( $NI$ ) which are spaced a coil radius ( $a$ ) apart, is

$$B_z(\xi) = (\mu_0 NI/2a)\{[1 + \xi^2]^{-3/2} + [1 + (\xi + 1)^2]^{-3/2}\} \quad \text{Eq. B-16}$$

where  $\xi = z/a$  and is measured from the center plane of the downstream coil.

One can show that for the Helmholtz coil if  $\xi = 0.3278$  then

$$(dB_z/d\xi)/B_z = -1$$

Eq. B-17

Figure B-6 compares the centerline exit magnetic fields of the solenoid and the Helmholtz coil. The downstream coil of the Helmholtz coil is located at  $\xi = z/a = -0.3278$  upstream of the exit of the solenoid,  $\xi = z/a = 0$ , and the magnetic field strengths have been set equal at this location. The resulting magnetic field divergence of the solenoid and the Helmholtz coil are essentially identical. This amount of field divergence is in the range which has been shown to be attractive for acceleration of a plasma, Ref. A-3, as discussed in the performance section of this report (Appendix A).

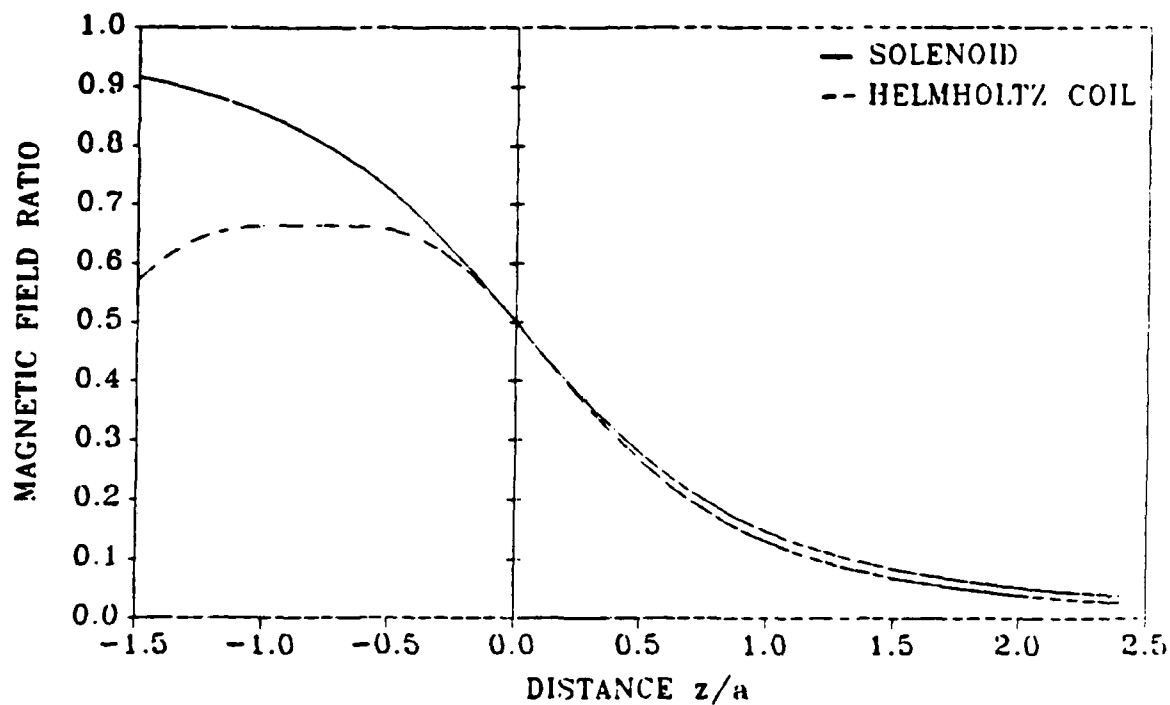


Fig. B-6 - Exit Field of a Solenoid and Helmholtz Coil  
with Equal Fields at  $z/a = 0$

#### REFERENCES APPENDIX B

B-1. Reitz, J. R., and Milford, F. J., Foundations of Electromagnetic Theory. Addison - Wesley Publishing Company, Inc., Reading, MA, 1960.

B-2. Spitzer, L. Jr., Physics of Fully Ionized Gases. Interscience Publishers, Inc., New York, N.Y., 1956.

B-3. Rose, D. J., and Clark, M. Jr., Plasma and Controlled Fusion. M.I.T. Press, Cambridge, MA, March 1965.

## APPENDIX C - MAGNETIC FIELD REQUIREMENTS FOR PLASMA CONTAINMENT

### C-1 - MINIMUM MAGNETIC FIELD WITH SHEAR TO CONTAIN A PLASMA

As indicated in Ref. C-1 (p.353), a necessary condition for stability of a cylindrical plasma with a radial pressure gradient,  $dp/dr$ , is

$$\left[ \mu_0 / B_{z0}^2 \right] \frac{dp}{dr} + \frac{r}{4} \left[ \frac{1}{b} \frac{db}{dr} \right]^2 \geq 0 \quad \text{Eq. C-1}$$

where  $1/b$  is the pitch of the magnetic lines.

The pitch of the magnetic lines is the distance  $z$  needed in Eq. B-8 for  $\phi$  to equal  $2\pi$ . Therefore:

$$1/b = 6\pi^2 B_{z0}^2 / (C^2 \lambda r^2) \quad \text{Eq. C-2}$$

substituting Eq. C-2 into C-1 and rearranging yields:

$$(B_{z0}^2 / 2\mu_0) (1/r) \geq - dp/dr \quad \text{Eq. C-4}$$

Interestingly this is not a function of the ratio magnitude of the shear to axial field  $(C/B_{z0})$ , but only of the fact that the

field has shear (i.e.  $db/dr > 0$ ).

If one assumes that the plasma pressure distribution is parabolic then

$$p = p_{\max} [1 - (r/r_{o-p})^2] \quad \text{Eq. C-5}$$

if  $p=0$  at  $r=r_{o-p}$  the outside radius of the plasma. Substitution of Eq. C-5 into Eq. C-4 then yield:

$$B_{zo}^2 / (2\mu_0) \geq 2p_{\max} \quad \text{Eq. C-6}$$

That is the magnetic pressure of the applied axial field must be greater than twice the maximum plasma pressure or greater than four times the average plasma pressure.

#### C-2 - MAGNETIC ENERGY OF A TOROIDAL PLUS SHEAR MAGNETIC FIELD

Define  $B_{zo}$  as the magnetic field at the center of a toroidal solenoid of major radius  $A$ , Eq. B-5. If three sets (six windings) of helical coils with opposing current flow ( $I_s$ ) are placed inside the toroidal coil, the resulting magnetic field components inside the torrus are given by Eqs. B-5, B-8 and B-9.

The magnetic field energy is:



$$B^2/(2\mu_0) = [B_z^2 + B_r^2 + B_\theta^2]/(2\mu_0) \quad \text{Eq. C-7}$$

Substituting Eqs. B-5 and B-8 yields:

$$B^2/(2\mu_0) = B_{z0}^2 \left[ \left( 1 + \frac{r}{A} \cos \theta \right)^{-2} + \left[ \frac{C}{B_{z0}} \right]^2 r^4 \right] \quad \text{Eq. C-8}$$

Clearly the minimum magnetic energy at any radius  $r$  will be at  $\theta=0$  since this maximizes  $\cos \theta$ . Thus, one obtains, by differentiation, the following condition for minimizing the magnetic energy:

$$0 = -2(1 + r_m/A)^{-3}/A + 4(C/B_{z0})^2 r_m^3 \quad \text{Eq. C-9}$$

Where  $r_m$  denotes the radius of the minimum magnetic energy.

Rearranging and substituting Eq. B-9 yields:

$$I_s/aB_{z0} = \frac{5.893 \times 10^5 (a/A)^{1/2} (a/r_m)^{3/2}}{[1 + (r_m/a)(a/A)]^{3/2}} \quad \text{Eq. C-10}$$

Figure C-1 shows how the quantity  $I_s/aB_{z0}$  varies as a function of  $r_m/a$  for various values of  $a/A$ . Since for a given  $a$  and  $B_{z0}$  the required  $I_s$  would be unbounded to minimize the magnetic energy at zero radius, the required  $I_s/aB_{z0}$  strongly decreases with  $r_m/a$  and by comparison is a much weaker increasing function of  $a/A$ .

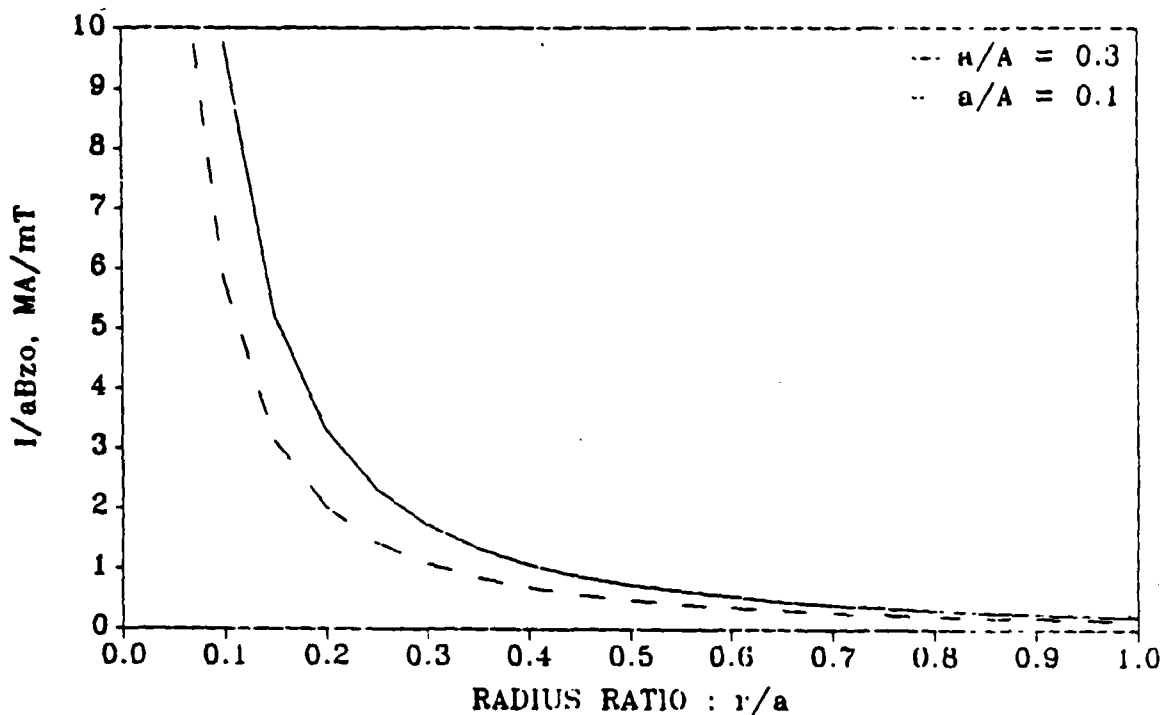


Fig. C-1 - Dimensionless Shear Coil Current as a function of the Dimensionless Radius of Minimum Magnetic Energy.

### C-3 - REQUIRED TWIST IN A TOROIDAL FIELD

Combining Eqs. B-8 and B-9 yields that the angle of twist,  $\phi$ , due to shear field coils with a pitch  $\lambda$  is

$$\phi = (9\mu_0^2 / \pi^2) (r/a)^2 (\lambda/a) (I_s/aB_{z0})^2 (z/a) \quad \text{Eq. C-11}$$

In half of a torrus of major radius  $A$  the twist would be given by  $z = \pi A$  in Eq. C-11. To permit current to flow along field lines to short out the electric field which could cause drift accross the toroidal field, the field twist angle must be greater than 180 degrees ( $\phi = \pi$ ) in the half toroidal field.

Therefore the following minimum condition for stability can be

derived from Eq. C-11:

$$I_s / aB_{z0} = 0.4702 \times 10^6 (\pi A / \lambda)^{1/2} (a/A) / (r/a) \quad \text{Eq. C-12}$$

Where  $\lambda / \pi A$  is the number of shear coil pitches in one half the major circumference of the torrus. Clearly the condition of Eq. C-12 cannot be met for very small  $r/a$  with a finite current  $I_s$ .

Equation C-12 is plotted in Fig. C-2 for two values of  $a/A$  and  $\pi A / \lambda$  equal to one. Comparing Figs. C-1 and C-2 shows that for any  $r/a$  the current  $I_s$  required to meet the minimum twist condition, Eq. C-12, is much less than the current  $I_s$  required to minimize the magnetic energy at that  $r/a$ . Thus, the minimum twist condition will be met at a radius of approximately  $1/3$  to  $1/2$  of the radius of minimum magnetic energy,  $r_m$ , and at  $r_m$  the magnetic twist in the half torrus will be approximately  $4$  to  $9\pi$ .

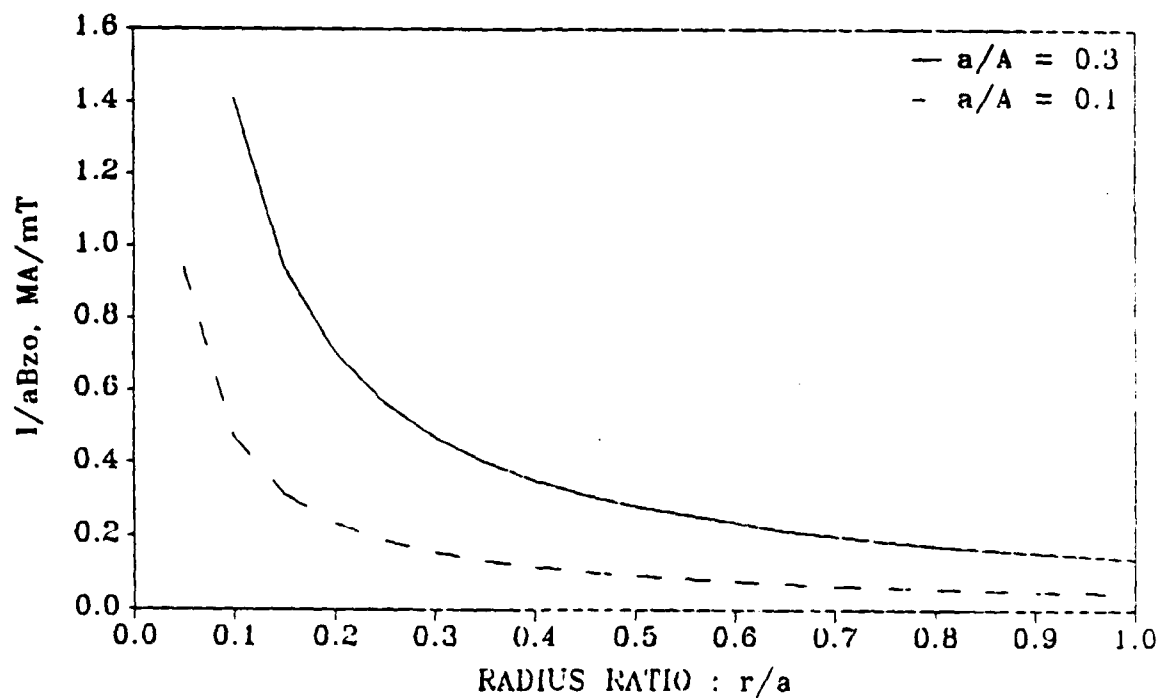


Fig. C-2 - Dimensionless Shear Coil Current Required for 180 Degree Field Twist in a Half Torus as a Function of Dimensionless Minor Radius.

#### REFERENCES APPENDIX C

C-1. Rose, D. J., and Clark, M. Jr., Plasma and Controlled Fusion. M. I. T. Press, Cambridge, MA, March, 1965.

## APPENDIX D - THRUSTER HEAT BALANCE AND PERFORMANCE CALCULATIONS

The thruster power balance and performance, as discussed in the section entitled thruster parameters and performance, was calculated using a commercially available spreadsheet program: "Smart". Table D-1 illustrates the spreadsheet and the thruster parameters for the nominal design case.

The parameters in rows 2 thru 6 are self explanatory constants used in the calculation. The quantities in rows 7 and 8 indicate if the shear coil radiation is from the sides (therefore proportional to coil height,  $H$ ), and, or from the top (therefore proportional to coil width,  $w$ ). The present design assumes radiation only from the coil sides.

The parameters from row 10 and down of the spreadsheet are defined in Table D-2 in the order in which they appear in Table D-1. The values shown in column 2 in table D-1 are in S.I. units. The values of parameters in column 3 are in inches and degrees F except for the quantities in column 3 row 45 and row 72. In these cases the values in column 3 are the specified desired value of  $Rho$  and  $Isp$  and are used in the calculation of the respective quantities  $Rho$  and  $Isp$ .

Quantities determined by explicit functions have their

equations contained in the spreadsheet cell. The calculation of the quantities  $I_s$ ,  $T_c$ ,  $P_s$ , and  $P_c$  (rows 36-39) and  $r_{min}$  (row 43) require iteration and are therefore determined by separate subroutines.

Calculation of a parametric case is accomplished by first inserting the values of the dependent and desired parameters in columns 2 & 3 of the spreadsheet and then executing a program entitled rho-pb. This program makes an initial guess at the coil temperature then executes the spreadsheet and the other two subroutines to calculate the value of rho, row 45. It then compares the value of rho with the desired value and modifies the coil temperature until the rho converges to the desired value. It then reexecutes the spreadsheet to obtain the final set of values for the parametric case. The program then inserts a blank row in column 4 of the spreadsheet and copies the results of the calculations in column 2 to column 4.

One can then change one of the independent parameters of the thruster and reexecute the program rho-pb to calculate another parametric case. The result of each parametric case is contained in a column of the spreadsheet. As more cases are calculated the spreadsheet just increases in its number of columns. The "Smart" program is capable of handling a spreadsheet with up to 999 columns so all the parametric cases can be contained in one spreadsheet and maintained in a single computer file.

Row\Column	1	2	3	4	5	6
1	TABLE D-1 - THRUSTER POWER BALANCE & PERFORMANCE PARAMETERS					
2	Resistivity (293K) & coef/deg.,K					
3	Cu	1.690E-08	3.930E-03			
4	Al	2.830E-08	3.900E-03			
5	S. Boltz. Con.		5.670E-08			
6	Permeability		1.257E-06			
7	Rad-H:0/1	1.000E+00				
8	Rad-w:0/1	0.000E+00				
9						
10	Bzo,T	3.000E-02				
11	A, m	1.100E-01	4.331E+00			
12	t tube, m	1.651E-03	6.500E-02			
13	r-i-s, m	2.540E-02	1.000E+00			
14	H-s, m	9.906E-03	3.900E-01			
15	t-s, m	2.540E-04	1.000E-02			
16	clearance	2.994E-03	1.179E-01			
17	N twists	1.000E+00				
18	f-theta-s	3.333E-01				
19	emis-s	9.500E-01				
20	f-s	9.500E-01				
21	r-c-c, m	7.000E-02	2.756E+00			
22	(r-f/r-c)c	8.000E-01				
23	r-o-c	7.500E-02	2.953E+00			
24	t-c,m	3.810E-04	1.500E-02			
25	L-n, m	5.335E-02	2.100E+00			
26	f-c	9.500E-01				
27	T-s,K	6.733E+02	7.520E+02			
28	ohm-m, -s	4.216E-08				
29	emis-c	9.500E-01				
30	a-s, m	3.035E-02	1.195E+00			
31	w-s, m	7.763E-03	3.056E-01			
32	L-s, m	3.947E-01	1.554E+01			
33	C, Ps/Is2	1.477E-03				
34	C,Is2,T4	5.408E+05				
35	C,Pc	1.320E+02				
36	Is, A tot	5.003E+02				
37	T-c, K	5.147E+02	4.665E+02			
38	P-s, W	3.697E+02				
39	P-c, W	2.460E+02				
40	P-n, W	5.604E+01				
41	P tot, W	6.717E+02				
42	C, r-min	3.356E+02				
43	r-min,m	1.781E-02	7.013E-01			
44	r-min/r-is	7.013E-01				
45	rho	7.500E-01	7.500E-01			
46	r-i-c, m	3.830E-02	1.508E+00			
47	r-f-c, m	5.600E-02	2.205E+00			
48	a-c, m	5.335E-02	2.100E+00			
49	N-s	3.900E+01				
50	I-s, A	1.283E+01				

TABLE D-1 - THRUSTER POWER BALANCE & PERFORMANCE PARAMETERS  
(CONCLUDED)

Row\Column	1	2	3	4	5	6
51	V-s. V	2.482E+01				
52	M-c	4.433E+02				
53	I-c. A	1.950E+01				
54	V-c. V	1.261E+01				
55	V-n. V	2.164E+00				
56	t-n. m	2.261E+01	1.056E+02			
57	Area-c. m2	1.592E+02	2.466E+03			
58	t-f-t. m	2.032E+03	8.000E+02			
59	t-f-n. m	5.080E+03	2.000E+01			
60	noz. kg/m3	2.300E+03				
61	M-s. kg	1.796E+00				
62	M-c. kg	7.291E+00				
63	M-n.s. kg	4.566E+00				
64	M coils. kg	1.436E+01				
65	M tube. kg	8.159E+01				
66	M-f-t.s. kg	7.248E+02				
67	a-e-n. m	3.103E+02	1.222E+00			
68	M noz.s. kg	1.606E+01				
69	M-f-n.s. kg	3.302E+01				
70	M tot. kg	1.731E+01				
71	V-arc. V	5.000E+02				
72	Isp-l. s	2.575E+03	2.900E+03			
73	beta	5.000E+02				
74	flow c/a	3.000E+02				
75	Q	2.209E+03				
76	kTe/e. V	1.207E+01				
77	ion cost. V	2.876E+01				
78	Eff-arc	8.738E+01				
79	Flow-a/P-a	2.741E+09				
80	Flow-a. kg/	1.174E+05				
81	P arc. W	4.283E+03				
82	I arc. A	8.566E+00				
83	Isp. s	2.500E+03				
84	Eff	7.333E+01				
85	P tot. W	4.955E+03				
86	P/anode. W	1.217E+02				
87	T. N	2.964E+01	6.664E+02			
88	Flow. kg/s	1.209E+05				



TABLE D-2 - POWER BALANCE AND PERFORMANCE PARAMETERS

Bzo,T:	Is the maximum center line containment field
A, m:	Is the major radius of the thruster's containment tube
t tube, m:	Is the thickness of thruster's containment tube
r-i-s, m:	Is the outside radius of the containment tube
H-s, m:	Is the height of the shear coil
t-s, m:	Is the thickness of the shear coil turns
clearance:	Is the distance between the shear and containment coils
N twists:	Is the number of times a shear coil winding rotates about the containment tube while going around the major circumference of the containment tube
f-theta-s:	Is the fraction of the circumference of the containment tube filled with shear coil windings
emis-s:	Is the emissivity of the shear coil
f-s:	Is the packing fraction of the shear coil
r-c-c, m:	Is the maximum radius of containment coil current
(r-f/r-c)c:	is the ratio of r-f-c to r-c-c
r-o-c:	Is the outside radius of the containment coil turn
t-c,m:	Is the thickness of the containment coil turn
L-n,m:	Is the length of the thruster's nozzles
f-c:	Is the containment coil packing fraction
T-s,K:	Is the temperature of the shear coil
ohm-m,-s:	Is the resistivity of the shear coil
emis-c:	Is the emissivity of the containment coil
a-s,m:	Is the effective radius of the shear coil

TABLE D-2 - POWER BALANCE AND PERFORMANCE PARAMETERS (CONTINUED)

W-s,m:	Is the width of the shear coil winding
L-s,m:	Is the average length of a shear coil winding
C,Ps/Is2:	Is a constant in calculating shear coil power
C,Is2,T4:	Is a constant in calculating shear coil current
C,Pc:	Is a constant in calculating containment coil power
Is,A tot:	Is the total ampere turns in a shear coil winding
T-c,K:	Is the temperature of the containment coil
P-s,W:	Is the power in the shear coils
P-c,W:	Is the power in the containment coil
P-n,W:	Is the power in the nozzle coils
P tot,W:	Is the sum of the coil powers
C, r-min:	Is a constant in calculating the radius of minimum magnetic energy density
r-min,m:	Is the radius of minimum magnetic energy density
r-min/r-is:	Is the ratio of r-min to r-i-s
rho:	Is the ratio of r-min to the inside radius of the containment tube
r-i-c,m:	Is the inside radius of the containment coil
r-f-c,m:	Is the radius at which the containment coil is cut flat
a-c,m:	Is the effective radius of the containment coil
N-s:	Is the number of shear coil turns
I-s,A:	Is the shear coil current
V-s,V:	Is the shear coil voltage
N-c:	Is the number of the containment coil turns

TABLE D-2 - POWER BALANCE AND PERFORMANCE PARAMETERS (CONTINUED)

I-c,A:	Is the containment coil current
V-c,A:	Is the containment coil voltage
V-n,A:	Is the nozzle coil voltage
t-n,m:	Is the nozzle coil turn thickness
Area-c,m <sup>2</sup> :	Is the area of a containment coil turn
t-f-t,m:	Is the thickness of the containment tubes flange
t-f-n,m:	Is the thickness of the nozzle flange
noz. kg/m <sup>3</sup> :	Is the density of the nozzle material
M-s,kg:	Is the mass of the shear coil
M-c,kg:	Is the mass of the containment coil
M-n.s,kg:	Is the mass of the nozzle coils
M coils,kg:	Is the sum of the masses of the shear, containment, and nozzle coils times 1.10 to allow for structure
M tube,kg:	Is the mass of the containment tube
M-f-t.s,kg:	Is the mass of the containment tube flanges
a-e-n,m:	Is the exit radius of the thruster's nozzles
M noz.s,kg:	Is the mass of the thruster's nozzles
M-f-n.s,kg:	Is the mass of the thruster's nozzle flanges
M tot,kg:	Is the thruster mass the sum of the above plus 5%
V-arc,V:	Is the thruster discharge voltage
Isp-I,s:	Is the ideal specific impulse of the thruster (not including cathode mass flow)
beta:	Is the ratio of the plasma pressure to the magnetic pressure of the containment field at the exit of the thruster's nozzle

TABLE D-2 - POWER BALANCE AND PERFORMANCE PARAMETERS (CONCLUDED)

flow c/a:	Is the ratio of the cathode mass flow to that of the sum of the two anodes
Q:	Is a quantity used in thruster performance calculations
$kT_e/e, V$ :	Is the plasma electron temperature inside the anodes
ion cost, V:	Is the cost of producing an ion in the thrusters discharge
Eff-arc:	Is the efficiency of the discharge not including the mass flow lost by the cathode or the coil power
Flow-a/P-a:	Is the ratio of the mass flow of the anodes in kg/s to the discharge power in W
Flow-a, kg/:	Is the sum of the mass flow of the two anodes kg/s
P arc, W:	Is the arc power
I arc, A:	Is the total arc current to both anodes
Isp, s:	Is the specific impulse of the thruster including the mass flow of the cathode
Eff:	Is the overall thruster efficiency including both cathode mass flow and the power of all the coils
P tot, w:	Is the total input of power to the thruster including both the discharge and all coils
P anode, W:	Is the power loss that must be radiated by each anode
T, N:	Is the overall thrust of the thruster
Flow, kg/s:	Is the total mass flow of the thruster